Waveguide Electrooptic Modulators

ROD C. ALFERNESS

Invited Paper

Abstract—**We give a tutorial review and brief summary of the present status of waveguide electrooptic modulators.**

I. Introduction

RESEARCH ON waveguide modulators is now in a rather advanced stage. The evolution to application in such areas as optical communication and high-speed signal processing seems to be imminent. Problem areas such as insertion loss and fiber-waveguide coupling are being addressed with increasingly promising results. Very wide-band modulators have been demonstrated. Promising applications such as analog to digital conversion are being pursued. In this paper we present here a semitutorial review of the operating principles and general design considerations for high-speed waveguide electrooptic modulators. Space does not permit a cataloging of all work done on the many possible modulator configurations. Rather we emphasize basic considerations common to most electrooptic modulators, stress waveguide, and electrode design considerations for optimized performance and consider in detail the most promising modulator candidates. We consider only single-mode devices; to date no wide bandwidth multimode modulators have been demonstrated. For early work in this field and a more complete bibliography, the reader is referred to several previous review articles [1]–[6]. Modulators based upon the acoustic-optic and magnetooptic effects are discussed in the earlier reviews.

II. Background

Research on bulk optical modulators began shortly after the invention of the laser several decades ago. The work was motivated by the desire to tap the enormous potential bandwidth offered by optical carrier frequencies. The goal of efficient, high-speed modulators stimulated researchers throughout the world to seek better electrooptic materials and efficient device geometries. This effort, indeed, resulted in modulation bandwidths of 1 GHz. However, the goal of low drive power was more illusive.

With the rapid reduction of loss in glass fibers in the late 1960's, research on optical modulators received new stimulus and an important new direction. Waveguide modulators were investigated primarily because of their compatibility with fibers and because of the ultimate goal of integration. However, in addition, the drive power advantage of waveguide modulators over their bulk counterparts was quickly realized. Diffraction effects prohibit making bulk modulators with both the small lateral dimensions and long interaction length needed to achieve low drive power. Guided-wave devices do not have this limitation and thus offer the potential of very low drive power.

Manuscript received April 26, 1982; revised May 5, 1982.
The author is with Bell Laboratories, Holmdel, NJ 07733.

III. Dielectric Waveguides

To fabricate dielectric waveguides the refractive index of the guiding region must be greater than the index of its surround. Planar waveguides, which guide light in the vertical direction but provide no lateral confinement, have been made by sputtering, epitaxial layers, ion implantation, ion exchange, and diffusion. Substrate materials include glass, semiconductors—GaAs [7]–[9] and more recently InP—, and insulating electrooptic crystals primarily $LiNbO_3$ and $LiTaO_3$. The bulk of waveguide modulator work has been done with Ti-diffused lithium niobate [10] and GaAs waveguides. With epitaxial layers the necessary index difference can be achieved either by lattice matched growth of an epilayer with different composition than the substrate or by the same material with different doping level. The latter is possible because of the refractive index decrease proportional to carrier concentration. The former is generally more desirable for two reasons. Larger index changes are achievable with composition (bandgap) differences than by using doping level changes. Furthermore, in spite of the fact that the light is guided in the region of low carrier concentration, the evanescent penetration into a highly doped substrate can cause free carrier absorption loss.

For compatibility with fibers and for efficient modulation, strip waveguides are essential and here we consider only strip waveguide modulators. Several channel waveguide geometries are shown in Fig. 1. In the first, a mask is used to allow a dopant to enter the substrate only through a narrow (typically 3–10 μm) strip. This technique can be used with indiffusion, ion exchange, and ion implantation but is not compatible with liquid phase epitaxial growth with semiconductor substrates. The latter two structures, rib [8] and metal-clad waveguides [9], have been used with planar epilayer waveguides on GaAs. Typical mode profiles for a strip waveguide with air cover are shown in Fig. 2.

0018-9480/82/0800-1121$00.75

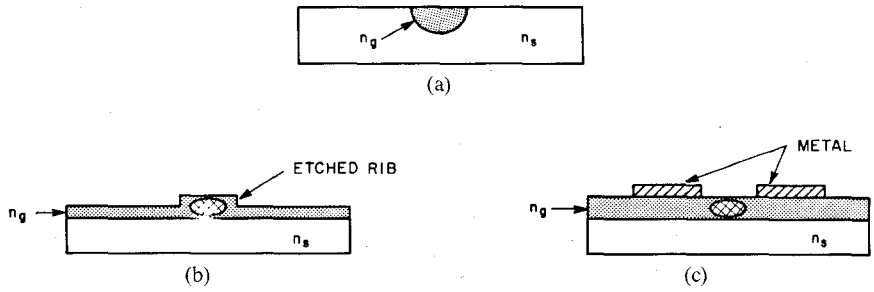

Fig. 1. Channel or strip waveguides. (a) Diffused, ion-exchanged or ion-implanted waveguide through opening in mask (not shown). (b) Rib waveguide etched into epitaxial planar waveguide. (c) Metal-clad waveguide.

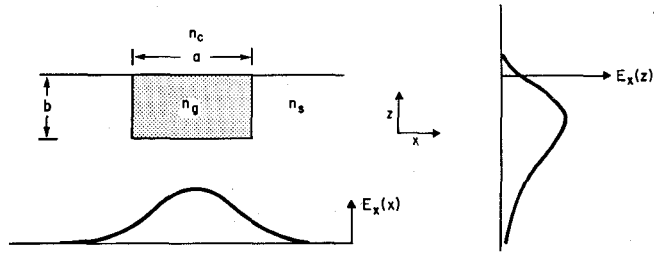

Fig. 2. Lateral and depth-mode profiles for air-clad channel waveguide.

TABLE I

	Δn	Loss (dB/cm)	w_{min}/λ	$n^3 r$ ($\times 10^{-6}$ μm/v)	$\frac{\epsilon_{eff}}{n^3 r}$ (arb)	N_m	$\lvert 1 - \frac{N_Q}{N_m} \rvert$
$LiNbO_3$	0.01-0.02	1, λ = 0.63 μm [13] 0.5, λ = 1.15 μm [7] 0.3, λ = 1.32 μm [14]	2.4	328	5.5	2	
GaAs	0.1	~4	0.6	49	25		< 0.3

For optimized modulator performance it is important to be able to achieve a small waveguide mode size. The minimum achievable mode size w_{min} can be written approximately as [11]

$$w_{min}/\lambda \sim 0.5/\sqrt{n_s \Delta n}\,. \tag{1}$$

$\Delta n = n_g - n_s$, where n_g is the refractive index of the guiding region and n_s is the substrate index. Typical values of Δn, resulting w_{min}/λ, and optical propagation loss for Ti:$LiNbO_3$ and GaAs waveguides are given in Table I. Using different substrate and epilayer composition with the ternary GaAlAs system offers a larger Δn than Ti:$LiNbO_3$ waveguides (Table I). Ion exchange techniques in lithium niobate offer a larger $\Delta n (\sim 0.1)$, but unfortunately provide guiding only for light of one polarization and for limited crystal orientations [12], [13]. The generally high propagation loss has been a serious disadvantage of semiconductor waveguides. Although there has been insufficient evidence, it appears these high losses are not fundamental and may be due to epilayer-substrate interface irregularities. Recently, relatively low-loss (~ 2.3 dB/cm) rib waveguides have been made with a GaAs epilayer grown through a narrow opening in a SiO_2 film on a GaAs substrate [14].

Waveguide modulators on semiconductor substrates offer the potential for monolithic integration with sources and electrical driver circuitry. InP is especially important because it is the most popular substrate for lasers that emit in the 1.3-μm–1.6-μm spectral region important for single-mode lightwave systems. Metal clad, [15] rib [16], and metal diffused [17] waveguides in InP have just recently been reported.

IV. Electrooptic Effect

The linear electrooptic (Pockels) effect provides a change in refractive index proportional to an applied electric field. The way in which this index change results in intensity modulation depends upon the device configuration which will be considered in detail later. Voltage V applied to the electrodes placed over or alongside the waveguide creates

an internal field of approximate magnitude $|E| \simeq V/G$ where G is the electrode gap. The applied field direction depends upon the crystal orientation and electrode placement. The electrooptic effect is described by a tensor relation. The linear change in the coefficients of the index ellipsoid due to applied fields (E_j) along the principle crystal axes is [18]

$$\Delta\left|\frac{1}{n_i^2}\right| = \sum_{j=1}^{3} r_{ij}E_j \tag{2}$$

or

$$(\Delta n)_i = -\frac{n^2}{2}\sum_{j=1}^{3} r_{ij}E_j \tag{3}$$

where $i=1,6$ and r_{ij} is a 6×3 electrooptic tensor. This relation can be contracted with the electrooptic tensor to write the six values of Δn as the elements of a symmetric 3×3 matrix. For example, for lithium niobate in the principal axes representation [18]

$$\Delta n_{ij} = \frac{-n^3}{2}\begin{vmatrix} -r_{22}E_y + r_{13}E_z & r_{22}E_x & r_{51}E_x \\ r_{22}E_x & r_{22}E_y + r_{13}E_z & r_{51}E_y \\ r_{51}E_x & r_{51}E_y & r_{33}E_z \end{vmatrix} \tag{4}$$

where n is either the ordinary n_o or extraordinary n_e value.

Utilization of the diagonal elements 11, 22, and 33 of the perturbed refractive index matrix results in an index change and, therefore, phase change for an incident optical field polarized along the crystallographic x, y, and z axes, respectively. For example, for an applied field along the z axis, the electrooptically induced index change for light polarized along the z direction which sees the extraordinary index and the strong r_{33} coefficient, is

$$\Delta n_e = -\frac{n_e^3}{2} r_{33}E_z. \tag{5}$$

The values of n^3r for the largest electrooptic coefficient for $LiNbO_3$ and GaAs are shown in Table I. (The results for InP are approximately the same as for GaAs. [19])

The off-diagonal elements of (4) represent electrooptically induced conversion or mixing between orthogonal polarization components. For example, an E_x field mixes the x and z optical polarization components through the r_{51} coefficient. Note that in the absence of an applied field, polarization along the principal axes is maintained for propagation along principal axes. Utilization of off-diagonal electrooptic elements is necessary for waveguide polarization modulation.

Voltage can be applied directly across a pair of electrodes on $LiNbO_3$ or $LiTaO_3$ which are insulating crystals. However, for semiconductor substrates like GaAs it is necessary to apply the field across a rectifying junction such as a Schottky barrier or p-n junction.

V. Modulator Voltage

The important characteristics of a waveguide modulator are: drive voltage required for a specific modulation depth, modulation bandwidth, and optical insertion loss. There are several modulator configurations for achieving intensity modulation from an electrooptically induced phase shift. While the required modulation voltage depends upon the modulator type, general conclusions concerning effectiveness of the applied field, modulation bandwidth, etc., can be made by considering the simple phase modulator. We consider separately devices on ferroelectric and semiconductor substrates.

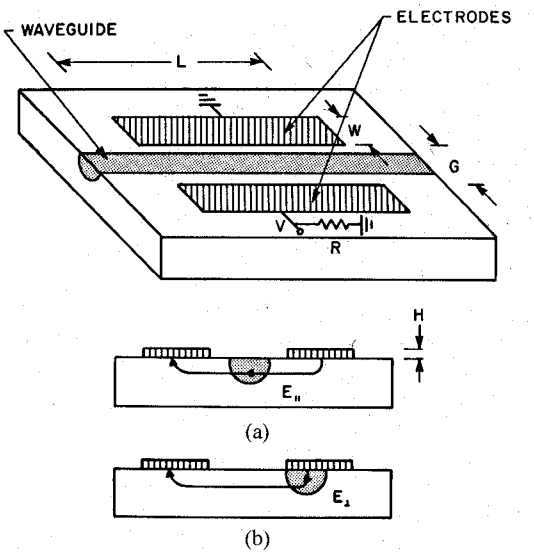

Fig. 3. Typical electrode configurations for waveguide modulators on insulating crystals. In (a) the horizontal field $E_\parallel$ is employed; in (b) the vertical field $E_\perp$ is used.

A waveguide phase modulator appropriate to Ti: $LiNbO_3$ is shown in Fig. 3. With electrodes placed on either side of the waveguide Fig. 3(a), the horizontal electric field $E_\parallel$ is used while the vertical electric field $E_\perp$ is employed with one electrode placed directly over the waveguide. In the latter case an insulating buffer layer such as SiO_2 or Al_2O_3 is required to eliminate loss due to the electrode, especially to the optical mode with polarization perpendicular to the substrate plane, the TM-like mode [20]. In either case, the crystal orientation should be chosen to use the largest electrooptic coefficient. For example, for lithium niobate the configuration of Fig. 3(a) offers utilization of the largest diagonal coefficient r_{33} for the TE mode (polarization in the plane of the substrate) for X-cut Y-propagating (or Y-cut X-propagating) crystals. The second configuration is appropriate for Z-cut orientation and provides maximum modulation for the TM mode.

The local electrooptically induced index change in either case is given by (4). However, neither the applied electric field nor the optical field is uniform. The effective electrooptically induced index change within a cross section of the optical mode can be written as

$$\overline{\Delta n}(V) = \frac{-n^3 r}{2}\frac{V}{G}\Gamma \tag{6}$$

where G is the interelectrode gap and Γ is the overlap integral between the applied electric field and the optical mode. Γ is given by

$$\Gamma = \frac{G}{V}\iint E|E'|^2\,dA \tag{7}$$

where E' is the normalized optical field distribution and E the applied electric field. In (6), the effective field is approximated by that of a simple parallel plate capacitor as in the bulk case and the optical field is assumed to be uniform. The correction factor from this simple model is given by the overlap integral. The total phase shift over the interaction length L is then

$$\Delta\beta L = \frac{-\pi n^3 r}{2}\Gamma\frac{V}{G}\frac{L}{\lambda}. \tag{8}$$

The exact phase shift required to achieve complete intensity modulation depends upon the modulator type. The modulation condition can be written in general as

$$|\Delta\beta L| = p\pi \tag{9}$$

where p, which depends upon the modulator type, is on the order of one. The voltage·length product required for modulation is thus

$$VL = \frac{p\lambda G}{n^3 r\Gamma}. \tag{9a}$$

The goal in modulator design is high modulation bandwidth with low drive voltage. We will show later that the achievable bandwidth also scales as $1/L$. Therefore, for a given electrooptic material and wavelength one tries to minimize VL by optimizing the geometric parameter G/Γ. To achieve a good overall modulator design it is essential to understand how Γ depends upon the electrode gap, waveguide mode size, the electric field component ($E_\perp$ or $E_\parallel$) employed, and the relative electrode-waveguide alignment.

Marcuse has recently analyzed the dependence of the field-mode overlap integral Γ upon the above parameters for the electrode structures of Fig. 3 (although semiinfinite electrodes were assumed) [21]. Similar analyses have also been recently reported by others [22], [23]. The waveguide mode dimensions ($w_\parallel$, and $w_\perp$ are the mode $1/e$ intensity full width and depth, respectively) serve as the characteristic lengths in the calculations of [21]. A mode profile typical of Ti:$LiNbO_3$ waveguides—Gaussian in width and Hermite Gaussian in depth (Fig. 2)—was assumed; however, the results are probably not very dependent upon the exact mode shape. Several general conclusions with respect to the influence of the alignment between the electrode and the optical mode upon the overlap integral can be made from the results of [21]. Most importantly, for electrode gap G comparable or only slightly larger than the mode size w, the optimum electrode placement for the geometry of Fig. 3(a) is for each electrode to be placed symmetrically about the waveguide. For utilization of the vertical field, it is generally best to align the inner edge of one electrode over the inner edge of the waveguide mode. For these alignment conditions, the relative index change·mode width product versus normalized electrode gap ($G/w_\parallel$) is shown in Fig. 4(a) and (b) for the modulator configuration of Fig. 3(a) and (b), respectively. Results are shown for $w_\perp/w_\parallel$ equal to 1 and 0.5, the latter being characteristic of Ti:$LiNbO_3$ waveguides. Also shown in each case is the overlap integral Γ for $w_\perp/w_\parallel = 0.5$. The scale is the same

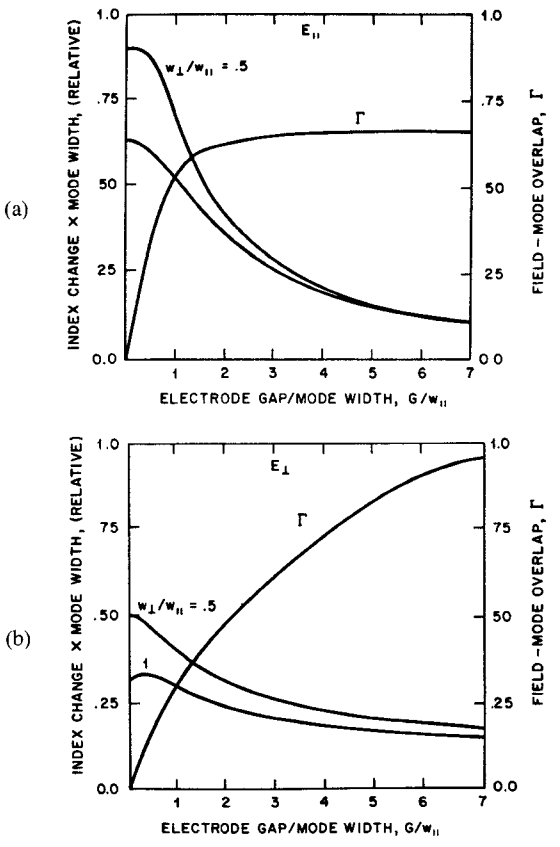

Fig. 4. Calculated index change·mode size ($w_\parallel$) (normalized by the optical waveguide) product and overlap parameter Γ versus normalized gap for $E_\parallel$ and $E_\perp$ fields (see Fig. 3). $w_\parallel$ and $w_\perp$ are the intensity $1/e$ full width and depth of the optical mode, respectively.

in each case and identical electrooptic coefficients are assumed.

Fig. 4 shows that although the induced index change continues to increase as the normalized gap $G/w_\parallel$ is decreased, the increase is relatively small for $G/w_\parallel < 0.5$. While the parallel field ($E_\parallel$) is more effective than the perpendicular component for small gap, the former also drops off more rapidly than the latter for large gap. In fact, for $E_\parallel$, the index change·mode size product drops off as $1/G$ but for $E\perp$ this product depends upon $1/\sqrt{G}$. As a result, the effective overlap parameter for electrodes placed over the waveguide is actually greater than 1 for large $G/w_\parallel$. This is apparently due to edge effects. This effect helps to explain the lower than expected drive voltage required for some reported waveguide modulators with relatively large electrode gap [24].

In either case, the overlap integral is zero for zero gap. Γ increases much more rapidly with increasing $G/w_\parallel$ for modulators that use $E_\parallel$ than for those that use $E_\perp$ but also saturates to a lower value. The small Γ for small $G/w_\parallel$ is unfortunate because it implies less efficient utilization of the electric field for small values of G for which V/G is large. Because the calculated quantity (left ordinate in Fig. 4) is the index change·mode size product, if $w_\parallel$ and $w_\perp$ are reduced then the e/o induced Δn increases as $1/G$, provided that fabrication techniques allow reducing G proportionately. Optimization of the induced index change

thus requires both minimizing the waveguide mode size and fabricating electrodes with a gap $G \lesssim 0.5 w_{\|}$, although for modulators that employ $E_{\perp}$ the latter requirement is not so critical.

VI. Bandwidth

The potential modulation bandwidth of waveguide modulators depends upon the electrode type and geometry and upon the substrate dielectric constant. Two types of electrodes—lumped and traveling wave—have been used for waveguide modulators.

A. Lumped Electrode

The modulation bandwidth for lumped electrodes can be examined using Fig. 3. The modulation bandwidth of the lumped electrode modulator (whose electrode length is small compared to the RF wavelength) is the smaller of the inverse of the optical or electrical transmit times or the time constant of the lumped circuit parameters. The latter is usually the more restrictive. The parallel resistor (Fig. 3) is used to allow broadband matching to the impedance of the driving source, typically 50 Ω. The capacitance per unit length for the electrode of Fig. 3 can be calculated using conformal mapping techniques. The result is [25], [26]

$$\frac{C}{L} = \varepsilon_{\text{eff}} \frac{K'(r_s)}{K(r_s)} \tag{10}$$

where $r_s = (2W/G + 1)^{-1}$ and $\varepsilon_{\text{eff}} = (\varepsilon_0/2)(1 + \varepsilon_s/\varepsilon_0)$. W is the electrode width, ε_s is the substrate RF dielectric, K is the complete elliptic integral of the first kind, and $K'(r_s) = K(\sqrt{1 - r_s^2})$. The capacitance per unit length for lithium niobate, where $\varepsilon_s = (\varepsilon_x \varepsilon_y)^{1/2}$, $\varepsilon_x = 28$ and $\varepsilon_y = 43$, is plotted in Fig. 5. Also shown is the potential bandwidth-length product where $\Delta f = 1/\pi RC$ and we assume $R = 50$ Ω.

Although C/L increases and consequently Δf decreases as G/W is decreased, both depend essentially only logarithmically on G/W. The electrical transit time cutoff frequency

$$f_t = \frac{c}{\pi \sqrt{\epsilon_{\text{eff}}} L} \tag{12}$$

is ~2.2 GHz·cm for lithium niobate, so there is no real advantage to $G/W \gtrsim 0.8$.

As discussed earlier, a small electrode gap is important to reduce the required drive voltage. This requirement together with that of small G/W for high bandwidth necessitates a relatively narrow electrode width. However, the reduction in electrode width is limited by two factors. First, W should not be much narrower than the waveguide width to insure good overlap of the electric and optical fields. Secondly, W must be sufficiently wide so that static electric resistance does not become the limiting factor in achievable bandwidth.

The limitation of static resistance to the achievable bandwidth for lumped electrodes has recently been examined theoretically [27]. There can be a dramatic reduction in modulation bandwidth for distributed static resistance of 5 Ω/mm or greater. However, for $R_E/L \lesssim 2$ Ω/cm, the bandwidth reduction due to distributed resistance can be estimated to be $\lesssim 20$ percent even for electrode length as long as 1 cm. For an electrode area (width × thickness) of 20 μm², the theoretical resistance per unit length ($R_E/L = \rho/A$, where ρ is the resistivity, and A is the electrode cross-sectional area) for gold (or approximately for Al) and copper are ~2 and 1.7 Ω/mm, respectively. Assuming an interelectrode gap of 3 μm, a G/W of 0.5 requires an electrode width of 6 μm. In this case, an electrode thickness of ~3 μm would be required to keep $R/L \lesssim 2$ Ω/mm. However, C/L changes only slowly with G/W. Therefore, even for a maximum electrode thickness of 0.5 μm which would necessitate an electrode width of 30 μm to minimize resistance effects, the potential $\Delta f_{RC} \cdot L$ would be only reduced from 2 GHz·cm to ~1.5 GHz·cm. (Fig. 5, $G/W = 0.1$).

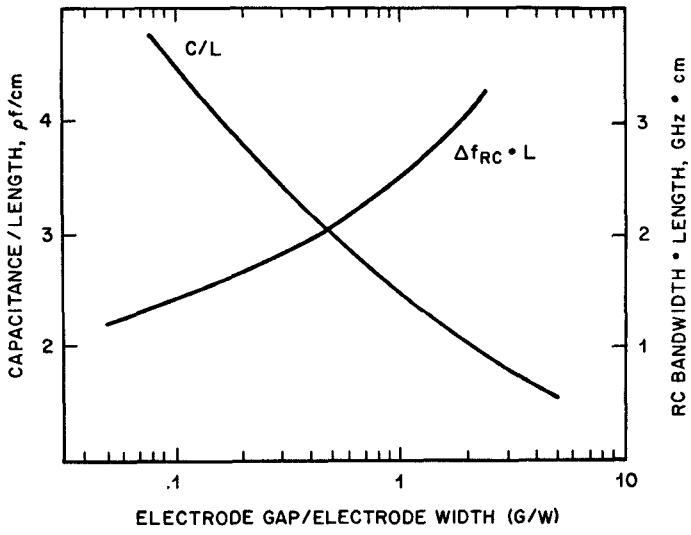

Fig. 5. Calculated capacitance per unit length for symmetric strip electrodes on lithium niobate versus the gap/width ratio. Also shown is the calculated RC bandwidth length product for a lumped modulator assuming $R = 50$ Ω.

The required modulation voltage scales inversely with length as does, in the absence of electrode resistance, the modulation bandwidth. Thus, increased bandwidth can be achieved at the expense of drive voltage by simply decreasing the device length. The appropriate modulator figure of merit is thus the voltage/bandwidth ratio. This figure of merit is generally more useful for comparing modulators than the power-per-unit bandwidth frequently used to characterize modulators, especially bulk devices. Because Δf depends upon the terminating resistance (R), it must also be specified. The required drive power, which is important for systems considerations, can then be calculated. For a given modulator, one can tradeoff drive power for bandwidth by changing R. The latter can be arbitrarily decreased by increasing L. From (9a) and (10) (assuming the capacitance limit) the voltage/bandwidth ratio is

$$V/\Delta f = \pi R \left(\frac{\varepsilon_{\text{eff}}}{n^3 r} \right) (p\lambda) \left(\frac{G}{\Gamma} \frac{K'(r_s)}{K(r_s)} \right) \tag{13}$$

where we have separated the material constants, modulator type, wavelength, and geometric dependence.

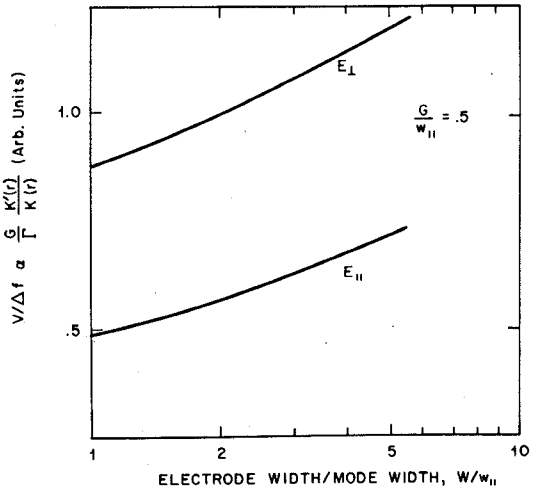

Fig. 6. Calculated increase in voltage/bandwidth ratio due to larger than optimum electrode width.

The geometry dependence of the voltage/bandwidth ratio, which is the last term in (13), can be calculated using the results of Figs. 4 and 5. As the electrode gap is reduced, $V/\Delta f$ decreases because the increase in C/L (Fig. 5) is less rapid than the decrease in the required voltage (Fig. 4). This is true for $G/w_{\|} \gtrsim 0.5$. Further reduction in G increases the capacitance/length without an appreciable increase in the induced index change. As a result, $V/\Delta f$ is minimum for $G/w_{\|} \simeq 0.5$ and $G/W \simeq 0.5$. However, because C/L is essentially logarithmically dependent upon G/W, the electrode width can be increased from its optimum value without severe reduction in $V/\Delta f$. This is shown in Fig. 6 where $V/\Delta f$ is calculated from the results of Figs. 4 and 5, assuming $G/w_{\|} = 0.5$ and $w_{\perp}/w_{\|} = 0.5$. A wider than optimum electrode width may be necessary if thick electrodes cannot be fabricated.

The results of Fig. 6 also indicate a significant advantage in $V/\Delta f$ for modulators which employ the parallel electric field. This advantage results entirely from the better overlap for small G exhibited by $E_{\|}$ compared to $E_{\perp}$ (Fig. 5). For the condition for minimum $V/\Delta f$ ($G/w_{\|} \sim 0.5$), $\Gamma_{\|} \sim 0.3$ while $\Gamma_{\perp} \sim 0.2$.

For the geometrical parameters to optimize $V/\Delta f$, the minimum achievable effective gap is limited by the minimum waveguide mode size. From the condition $G/w_{\|} = 0.5$ and (1)

$$G_{\min} \sim \frac{0.25\lambda}{\sqrt{n_s \Delta n}}. \tag{14}$$

For lithium niobate, assuming $\Delta n \simeq 0.01$, $G_{\min} \simeq 1$ μm and 2 μm for $\lambda = 0.63$ μm and 1.3 μm, respectively. If (14) is used in (13), as is the optimum value of $K'(r_s)/K(r_s)$ ($= 2$ for $G/W = 0.5$), we find

$$(V/\Delta f)_{\min} \simeq 0.5\pi R \left(\frac{\varepsilon_{\text{eff}}}{n^{7/2} r \sqrt{\Delta n}} \right) \frac{p\lambda^2}{\Gamma} \tag{15}$$

where Γ is 0.3 or 0.2 for modulator employing $E_{\|}$ of $E_{\perp}$, respectively.

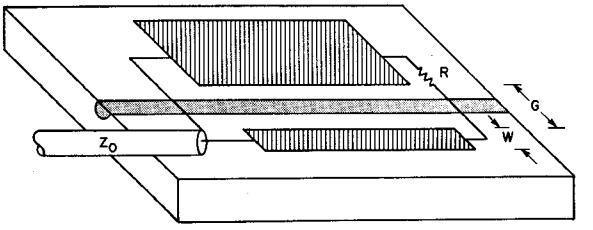

Fig. 7. Asymmetric coplanar strip traveling-wave electrode.

For optimum design, a material with large electrooptic coefficient, high refractive index, low dielectric constant, and capable of forming waveguides with large guide-substrate index difference are required. For lithium niobate assuming $p = 1$, and $R = 50$ Ω, that electrode resistance can be ignored, the approximate minimum value of $V/\Delta f$ for lumped modulators is ~ 0.5 V/GHz and 1.5 V/GHz for $\lambda = 0.6328$ μm and 1.32 μm, respectively.

(15) indicates that for optimum design $V/\Delta f$ scales as λ^2. However, for modulators where no attempt is made to minimize the waveguide mode size, the dependence upon λ is perhaps somewhere between linear and quadratic. In either case, a significant voltage penalty is paid between operation at visible wavelengths and the long wavelengths (1.3 μm to 1.5 μm) required for lightwave communication systems.

The results considered here assume an ideal modulator. Stray and lead capacitance have, for example, been ignored. To obtain this potential, good electrical packaging is very important.

B. Traveling Wave

The goal of the traveling-wave electrode, shown schematically in Fig. 7, is to make the electrode appear as an extension of the driving transmission line. As such, it should have the same characteristic impedance as the source and cable. In this case, the modulator speed is not limited by the electrode charging time but rather by the difference in transit time for the optical and modulating RF waves. The asymmetrical electrode structure in Fig. 7 has been used for traveling-wave modulators because of its low propagation loss, and good coupling to an external coax cable [28]. The capacitance per unit length for the asymmetric electrode can also be determined by conformal mapping techniques. The result is [29]

$$\frac{C}{L} = 2\varepsilon_{\text{eff}} \frac{K'(r_a)}{K(r_a)} \tag{16}$$

where $r_a = (2W/G + 1)^{-1/2}$. Calculated C/L versus G/W for lithium niobate is shown in Fig. 8. Also shown is the characteristic impedance

$$Z_0 = \left(\frac{cC}{\sqrt{\varepsilon_{\text{eff}}} L} \right)^{-1} \tag{17}$$

versus G/W, where c is the speed of light. For given G/W, C/L is higher for the asymmetric electrodes than for symmetric ones. From (16) and (17), to achieve a 50 Ω transmission line for an asymmetric coplanar strip on

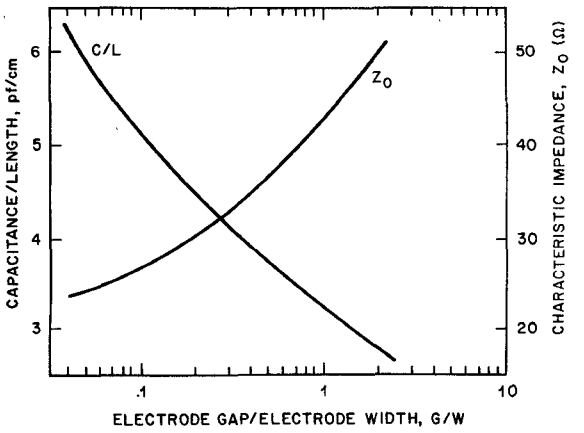

Fig. 8. Calculated capacitance/length and characteristic impedance for asymmetric coplanar strip on lithium niobate.

lithium niobate, a value of $G/W \simeq 1.7$ is required compared to $G/W = 0.6$ for the symmetric coplanar strip.

The required drive voltage is, of course, independent of the electrode type but the expected modulation bandwidth for the traveling-wave electrode is quite different from the lumped electrode. To examine the bandwidth limitation of traveling-wave modulators we assume the electrode impedance is matched to the connecting cable and source. The microwave drive signal is

$$V(z,t) = V_0 \sin\left(\frac{2\pi N_m}{\lambda_m} z - 2\pi f t\right) \tag{18}$$

where $N_m = \sqrt{\varepsilon_{\text{eff}}}$, λ_m and f are the microwave refractive index, free space wavelength and frequency, respectively. z is position along the electrode. For simplicity, we ignore microwave loss for the moment. The voltage seen at any point along the electrode by a photon that enters the waveguide at any time t_0 can then be written as

$$V(z,t_0) = V_0 \sin\left\{\frac{2\pi N_m f}{c}\left(1 - \frac{N_0}{N_m}\right) z - 2\pi f t_0\right\} \tag{19}$$

where N_0 is the effective index of the guided optical mode. Then, because the electrooptically induced phase shift $\Delta\beta$ is proportional to V, the integrated $\Delta\beta$ is

$$\int_0^L \Delta\beta(f)\, dz = \frac{\overline{\Delta\beta}\, \sin\left(\frac{\pi f L N_m \delta}{c}\right)}{\left(\frac{\pi f L N_m \delta}{c}\right)} \sin\left(2\pi f t_0 - \frac{\pi f L N_m \delta}{c}\right) \tag{20}$$

where $\overline{\Delta\beta} = -\pi n^3 r V_0 \Gamma L/\lambda G$ and $\delta = 1 - N_0/N_m$ is a measure of the velocity mismatch between the optical and microwave signals. For $N_0 = N_m$, the optical wave travels down the waveguide at the same speed as the microwave drive signal moves along the electrode and "sees" the same voltage over the entire electrode length. The integrated value of $\Delta\beta$ is proportional to $V_0 L$, and arbitrarily long electrodes can be used to reduce the required drive voltage with no frequency limitation. However, for $N_0 \neq N_m$, there is walk-off between the optical wave and microwave drive signal which results in a reduction, and for sufficiently large L or f, a complete cancellation of $\Delta\beta$. Thus, the sin(x)/x functional frequency response of (20). According to (20), the frequency for which the integrated value of $\Delta\beta$ is reduced by 50 percent from its value for $f = 0$ is

$$\Delta f \cdot L = \frac{2c}{\pi N_m \delta}. \tag{21}$$

Therefore, for given electrode length, the achievable bandwidth is critically dependent upon the mismatch between the optical and microwave velocities. The value of $N_m \Delta$ for lithium niobate and GaAs are listed in Table I. Based on this parameter GaAs offers significant advantage for traveling-wave modulators. According to (21) and the data in Table I, the expected $\Delta\beta$ frequency·length product for lithium niobate and GaAs are 9 GHz·cm and >60 GHz·cm, respectively. (Some authors define the bandwidth by the frequency for which the drive power must be doubled to maintain the modulation depth at low frequency [27].)

Electrode loss reduces the effective $\Delta\beta$ seen along the modulator length. Frequency independent loss can be compensated for by an increased driving voltage. However, if the loss depends upon f, as is generally the case, the frequency bandwidth is reduced. In either case, the figure of merit $V/\Delta f$ is increased from the ideal velocity mismatch limit.

For given electrode dimension, the high frequency microwave loss is determined by the skin depth and one expects a loss in dB/cm of $a = a_0 f^{1/2}$, where a_0 depends upon electrode conductivity and geometry. This frequency dependence has been verified experimentally [29]. Assuming no velocity mismatch, the effect of loss on the integrated $\Delta\beta$ is

$$\int_0^L \Delta\beta(z)\, dz = \frac{\overline{\Delta\beta_0}}{\alpha_m}\left(1 - e^{-\alpha_m L}\right) \tag{22}$$

where $\alpha_m = a/4.3$ converts from loss in dB/cm to an exponential-loss coefficient. Assuming a skin depth frequency dependent loss with $a_0 = 1$ dB/cm·GHz$^{1/2}$, a value achieved experimentally [29], and a 1.5-cm long electrode, the frequency for which the integrated $\Delta\beta$ is reduced by 50 percent relative to low frequency is ~10 GHz. This limit is somewhat less restrictive through comparable to the ~7-GHz bandwidth limit due to velocity mismatch for lithium niobate. For high frequency (>56 GHz), coax coupling loss may be as important as propagation loss.

If we ignore loss, the voltage/bandwidth ratio for traveling-wave electrode modulators is

$$V/\Delta f = \frac{\pi}{2C}\left(\frac{\varepsilon_{\text{eff}}\Delta}{n^3 r}\right)(p\lambda)\frac{G}{\Gamma} \tag{23}$$

where, if we further assume the mode-size limited minimum gap (14)

$$(V/\Delta f)_{\min} = \frac{\pi}{8C}\left(\frac{\varepsilon_{\text{eff}}\Delta}{n^{7/2} r \Delta f \sqrt{\Delta n}}\right)\frac{p\lambda^2}{\Gamma}. \tag{24}$$

Equation (24) is actually quite over-optimistic. To achieve

simultaneously an electrode impedance of 50 Ω and a small electrode gap needed to minimize $V \cdot L$, a very narrow electrode width is required. For example, for $G = 5$ μm, an electrode width of only 3 μm is necessary for $Z = 50$ Ω with an asymmetric electrode. As a result, researchers have used either narrow gap or 50-Ω electrodes but not both. Assuming a 50-Ω impedance source in both cases, the first approach allows more efficient use of the applied voltage but suffers a reduction in effective applied voltage due to impedance mismatch reflection and to the lower impedance. In the latter case, all the source-delivered microwave power is coupled onto the electrode but the large gap results in a less then optimum induced phase shift. A source with lower impedance can be used but because the important modulator parameter is voltage, for the same source power the applied voltage is $V_0 \sim \sqrt{Z_0}$.

For a specific comparison, we consider two electrodes of equal length and metal thickness, one with $W_1 = 20$ μm and $G_1 = 30$ μm and the other $W_2 = 20$ μm and $G_2 = 5$ μm. The characteristic impedances on lithium niobate (Fig. 8) are $Z_0 = 50$ Ω and 30 Ω, respectively. Because of their identical width and thickness, we assume the two electrodes have equal loss which for simplicity we assume is zero. If each electrode is terminated in its characteristic impedance the potential bandwidth in each case is equal [29] and is given by (21). Therefore, the relative $V/\Delta f$ is given simply by the ratio of required drive voltages. Assuming a 50-Ω source, an impedance matched power P_0 (source power) is delivered in the first case and only

$$0.9375P_0 = \left\{1 - \left(\frac{Z_L - Z_0}{Z_L + Z_0}\right)^2\right\} P_0$$

in the second case. Therefore, for the same source power, the delivered voltage in the two cases are $(V_1/V_2) = 1.33$. If we assume that the narrower gap corresponds to $G = 0.5\, w_{\parallel}$, then the ratios of electrooptically induced Δn for the two cases under equal drive voltage are (Fig. 4, with $w_{\perp}/w_{\parallel} = 0.5$) $\Delta n_1/\Delta n_2 = 0.56$ and 0.36 for $E_{\perp}$ and $E_{\parallel}$, respectively. Taking into account the difference in effective delivered voltage in the two cases, the ratios of actual induced Δn is $\Delta n_1/\Delta n_2 = 0.75$ and 0.5 or $(V/\Delta f)_1/(V/\Delta f)_2 = 1.33$ and 2 for $E_{\perp}$ and $E_{\parallel}$, respectively. Thus, there appears to be an advantage to using the smaller gap even if it means abandoning impedance matching.

In fact, for equal electrode width, the microwave loss may be somewhat larger for the narrower gap electrode [30], which would reduce the apparent advantage for the smaller gap electrode. The optimum traveling-wave electrode design, therefore, requires careful consideration of the geometry related tradeoffs between loss and the efficient utilization of the microwave voltage. The relatively large G/W ratio required for a 50-Ω coplanar strip on lithium niobate results from its large dielectric constant. The desire for small gap for modulators is in contrast to typical microwave integrated circuit applications. Further investigation into the microwave engineering of these structures may result in small gap, low-loss traveling-wave electrodes.

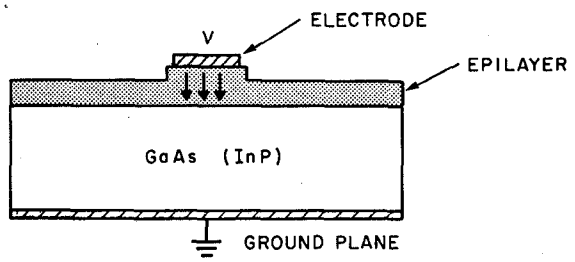

Fig. 9. Rib waveguide-electrode configuration for semiconductor waveguide modulator.

The traveling-wave electrode has a clear bandwidth·length advantage over the lumped electrode even for the velocity mismatch of lithium niobate. However, if electrode loss precludes simultaneous achievement of impedance matching and a small gap, the advantage in $V/\Delta f$ for a traveling-wave electrode over a small gap lumped electrode may be less substantial. For large gap use of $E_{\perp}$ is preferred.

For both lumped and traveling-wave electrodes, a metal thickness of 2–3 μm is desirable. Typically metallic electrodes are delineated by lift-off techniques. In this case, the metal thickness is limited to a fraction of the photoresist thickness generally $\lesssim 0.5$ μm; however, special techniques have been developed to increase this to ~1 μm [30], [31]. Lift-off provides the potential for very narrow electrode gap (~1 μm) [33]. Aluminum electrodes as thick as 3 μm have been fabricated by chemical etching but only for large gap, ~25 μm [24]. Both thick electrodes (3 μm) and relatively narrow gap (6 μm) have been achieved with plasma etching [29]. Other techniques such as reactive ion etching using a reactive CCl_4 gas, for example, may also prove useful in providing narrow width, low-loss electrodes [34].

C. Semiconductor Waveguide Modulators

A schematic drawing of an waveguide-electrode geometry appropriate to a GaAs or InP phase modulator is shown in Fig. 9. The electric field is developed across either a diffused p-n junction or Schottky barrier. In either case, the effective dimension is the depletion region d. d can be quite small, on the order of 1 μm. Furthermore, for the relatively large waveguide-substrate index difference achievable with epitaxial waveguides, a mode depth on the same order is possible. Thus, the geometric component $G/\Gamma = d/\Gamma$, of the voltage·length product in (9a) can be made small, approaching 1 μm. Indeed, by optimizing this geometric parameter, GaAs waveguide phase and polarization modulators with voltage·length products of ~1.1 V·cm for $\lambda = 1.06$ μm have been demonstrated [35]. This value is comparable to that for lithium niobate, in spite of the 6 to 1 advantage of the latter in the electrooptic figure of merit.

Because of the rectifying junction required for semiconductor waveguide modulators, the analysis for expected bandwidth is somewhat more complicated than for insulat-

ing substrates. For simplicity, the junction can be modeled as a simple parallel plate capacitor with electrode separation d. Then $C/L = \varepsilon_{\text{eff}}/d$, where, in this case, $\varepsilon_{\text{eff}} = \varepsilon_s$, which is ~ 13 for GaAs and InP. In fact, however, the depletion thickness generally depends upon the applied voltage for both the p-n junction and Schottky barrier [36]. As a result, the capacitance depends upon the drive voltage and for a time-varying signal parametric effects that result in harmonic distortion of the optical modulation might be expected. There are insufficient experimental results for high frequency GaAs modulators to assess the significance of such distortion. However, in early work on GaP modulators by proper waveguide fabrication such second-harmonic distortion was maintained below 5 percent, for modest modulation depth [37].

To date, no semiconductor waveguide modulators with traveling-wave electrodes have been reported. Because of the small velocity mismatch for both GaAs and InP, traveling-wave modulators on these substrates would appear very promising. The lower dielectric constant of GaAs and InP also allows a smaller G/W ratio for a given impedance than in lithium niobate. However, the fact that the junction capacitance depends upon voltage complicates the question of the microwave stripline transmission on these materials. This question and, perhaps more importantly, that of microwave loss in such structures requires considerable exploration. In addition, the typically large optical loss of semiconductor waveguides presently precludes the use of long modulators to take full advantage of the small velocity mismatch.

VII. Intensity Modulators

For most applications, optical intensity modulation is required and some means is necessary to convert the electrooptically induced phase modulation into intensity modulation. In bulk and early waveguide modulators, this was accomplished by placing linear polarizers with axis at $+45°$ and $-45°$ with respect to the substrate plane before and after the waveguide, respectively [4]. Because the TE and TM modes see different e/o coefficients, there is a voltage-dependent phase shift between them. They are effectively mixed by the output polarizer to produce intensity modulation. Unfortunately, external polarizers are required because there is no known way to make passive 45° waveguide polarizers.

Integrated intensity modulators have been made using a variety of waveguide structures. While space does not permit a survey of all of them, we briefly describe the most promising. The most popular are the directional coupler and interferometric modulators shown in Fig. 10. While we show the modulators with electrodes on the waveguides, the configuration of Fig. 3(a) can be used. In the switched directional coupler [38] (Fig. 10(a)), two identical strip waveguides are brought in close proximity over a length L. Because of the overlap in the evanescent fields of the two waveguides, light couples between them with a coupling coefficient per unit length κ, which depends upon the waveguide parameters, wavelength, and interwaveguide

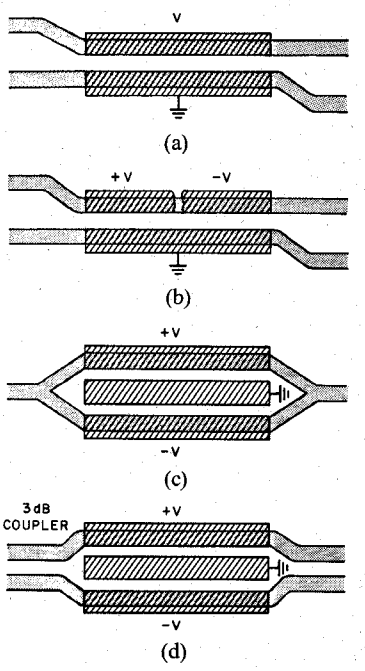

Fig. 10. Intensity modulators. (a) Switched directional coupler. (b) Reversed $\Delta\beta$ coupler. (c) Y-branch interferometer. (d) Mach–Zehnder interferometer.

separation [39], [40]. For an appropriate length, all the light entering in one waveguide can couple to the other. By electrooptically producing an index difference between the two waveguides, light which crosses over at different points along the directional coupler is no longer in phase and the net crossover efficiency can be made zero. The voltage-dependent crossover efficiency can be found by solving the well-known coupled-mode equations and is [41]

$$\eta = \frac{1}{1+\left(\frac{\Delta\beta}{2\kappa}\right)^2}\sin^2\left\{\kappa L\left(1+\left(\frac{\Delta\beta}{2\kappa}\right)^2\right)^{1/2}\right\}. \quad (25)$$

For $\Delta\beta = 0$, $\eta = 1$; for $\kappa L = m\pi/2$, m is an odd integer. A value

$$\Delta\beta L = m\pi\sqrt{4\left(\frac{n}{m}\right)^2 - 1}$$

where n is the first integer $> m/2$, is then required to make $\eta = 0$. Only two ports are required. $\eta(\Delta\beta L)$ is plotted in Fig. 11 for $\kappa L = \pi/2$ an $3\pi/2$.

It is clear from Fig. 11 and the formula above that to minimize the necessary $\Delta\beta L$ for 100 percent modulation, a single coupling length $l = \pi/2\kappa$ is desirable. Multiple coupling-length devices result in a significantly larger required $\Delta\beta L$. For $\kappa L = \pi/2$, the value of p ((9a)) for 100 percent intensity modulation is $\sqrt{3}$. Using the push-pull arrangement of Fig. 10(a), this is reduced to $p = \sqrt{3}/2$. By varying κ along the directional coupler length, the shape of the voltage response can be changed in an advantageous manner [42]. For example, the voltage response sidelobes (Fig. 11) can be significantly reduced.

Two difficulties of the switched directional coupler can be overcome with the reversed $\Delta\beta$ coupler of Fig. 10(b)

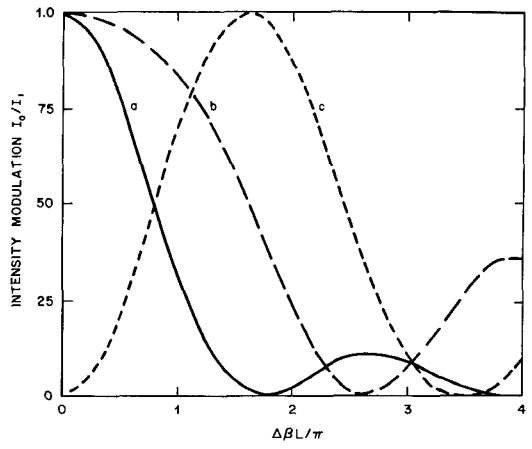

Fig. 11. Voltage $\Delta\beta$ response curves for: (a) switched directional coupler with $L=l$; (b) switched directional coupler with $L=3l$; and (c) reversed $\Delta\beta$ with $L=2l$. In all cases the curves are symmetrical in $\Delta\beta$.

[43], [44]. Here one electrode is split into two equal lengths driven with opposite polarity voltage. These problems are the fabrication difficulty with reproducibly making $\kappa L = n\pi/2$ to assure 100 percent crossover in the absence of voltage and the fact that a larger value of $\Delta\beta L$ (or p in (9a)) is required if L corresponds to multiple coupling lengths. The former is more critical for switching applications where low crosstalk for both switch states is required. For modulators $\kappa L \neq n\pi/2$ results in loss. The second problem is more critical. An appropriately small electrode gap is desirable to reduce drive voltage while this gap should be approximately equal to the interwaveguide gap to assure best $V/\Delta f$. However, for typical values of G, the transfer length l is small compared to the L required for acceptable low drive voltage [40]. In this predicament, the full advantage of lower V for longer L is not realized because p ((9a)) increases with L. However, for the reversed $\Delta\beta$ modulator, the required swing in $\Delta\beta L$ is $\sim\sqrt{3}\,\pi$ even if $L/l>1$. This is true provided that one uses a number of electrode sections equal to the approximate number of coupling lengths. The voltage response for an N (N even) section $\Delta\beta$ reversed modulator can be written as [43], [6]

$$\eta = \sin^2 \kappa_{\text{eff}} L \tag{26}$$

where

$$\kappa_{\text{eff}} = \frac{N}{L} \sin^{-1} \sqrt{\eta_s}\,. \tag{27}$$

η_s is the crossover efficiency of one section of length L/N given by (25). This response ((26)) is plotted in Fig. 11 for $N=2$ and $\kappa L = \pi$. With proper dc bias the swing in $\Delta\beta L$ for complete modulation is $\sim\sqrt{3}\,\pi$. Thus, $p=\sqrt{3}$ or $\sqrt{3}/2$ including the push-pull effect.

The Y branch [45] and balanced bridge [46] (Mach–Zehnder) modulators are shown in Fig. 10(c) and (d), respectively. The former has been especially popular because of its apparent simplicity. Both employ the same principle. An input wave, split into equal components, propagate over the two arms of the interferometer which are sufficiently separated to prohibit evanescent coupling between them. If no phase shift is introduced between the interferometer arms, the two components combine in phase at the output Y-branch 3-dB coupler and continue to propagate undiminished in the output waveguide. For the M–Z, no phase shift results in complete crossover at the output 3-dB coupler. For a π phase shift, the field distribution after the output Y-branch waveguide corresponds to the second-order mode which is not supported by the single-mode output waveguide. Light is radiated into the substrate and the transmitted light is a minimum. For the M–Z, the light exits from the input waveguide for $\Delta\beta L = \pi$. In either case, the transmission efficiency (if one monitors the crossover waveguide for the M–Z) is

$$\eta = \cos^2 \frac{\Delta\beta L}{2}\,. \tag{28}$$

For 100 percent intensity modulation, $\Delta\beta L = \pi$ is required, so $p=1$ (in (9a)). While the advantage of push–pull in $\Delta\beta$ can be achieved using the three electrode configuration shown in Fig. 10, the capacitance for this case, which is examined in [25] and [27], is nearly twice that of the two electrode structure of same dimension. As a result, the value of $V/\Delta f$ does not benefit greatly. A two electrode configuration with interelectrode gap equal to the rather large interwaveguide gap can be used to advantage if a large G is required for other considerations, but the large gap necessitates a relatively large drive voltage. This is true of the fastest reported TW modulator which will be discussed below. Alternately, a small-gap push-pull two electrode structure can be used for an interferometer with a small interwaveguide gap provided the evanescent coupling is eliminated. This has been achieved by etching [47] the substrate between two closely spaced waveguides and by mismatching [48] them by fabrication.

The M–Z, unlike the Y-branch interferometer, but like the two directional coupler devices, has the advantage of functioning as a switch as well as a simple on/off modulator. Thus, these devices are candidates for high-speed time division multiplexers which may be important devices to utilize the high bandwidth of single-mode fibers.

Three other promising waveguide modulators are the cutoff, total internal reflection (TIR), and polarization modulator. The first is simply a phase modulator in which the induced index change reduces the waveguide-substrate index so that guiding is eliminated and light radiates into the substrate [49]. It has the advantage of being simple. However, for low modulation voltage, the waveguide must be near cutoff which usually implies significant optical loss for the on ($V=0$) state.

The TIR switch/modulator shown in Fig. 12(b) uses the electrooptically induced index change to cause light incident in the top, upper waveguide (for example) to be reflected into the upper, right waveguide [50]. For $V=0$, most of the light remains in the incident waveguide. The value of voltage required for switching is [50]

$$\frac{V}{G} \sim \frac{1}{n^2 r} \left| \frac{\theta_i}{2} \right|^2 \tag{29}$$

where θ_i is the half angle between the waveguides. To reduce V, a small angle is desirable. However, the reduction in θ_i is limited by unwanted evanescent coupling in the region outside the electrode.

According to the switching condition of (29), V does not

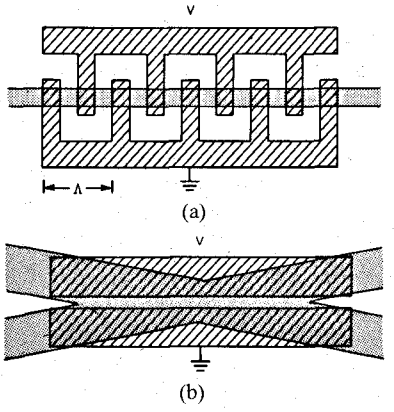

Fig. 12. (a) Phase-matched polarization modulator and (b) total internal reflection switch/modulator.

depend upon either the wavelength or electrode length. This point offers potential in decoupling the normally incompatible requirements of low voltage and large bandwidth common to the other modulators described.

A polarization modulator appropriate to lithium niobate is shown in Fig. 12(a). This modulator uses an off diagonal element of the electrooptic tensor ((4)) to convert incident TE- (TM) to TM- (TE) polarized light. A periodic electrode is shown in Fig. 12(a) because lithium niobate is birefringent and periodic coupling with a period Λ, such that [51], [52]

$$\frac{2\pi}{\lambda}|N_{TM}-N_{TE}|=\frac{2\pi}{\Lambda} \tag{30}$$

is required to effect efficient TE $\leftrightarrow$ TM conversion. For lithium niobate, the required period is $\Lambda=7$ μm and 18 μm for $\lambda=0.6$ and 1.3 μm, respectively. This coupling process is again described by the coupled-mode equations with $\Delta\beta=0$ (provided (30) is satisfied) so

$$\eta=\sin^2\kappa L \tag{31}$$

where

$$\kappa=\frac{\Gamma\pi}{\lambda}n^3r\frac{V}{G}. \tag{32}$$

For 100 percent polarization modulation, therefore, $p=1/2$, which is the lowest modulation condition of the devices considered. The capacitance of the interdigital structure of Fig. 12(a) is analyzed in (25). Although the total electrode length is greater than the interaction length, the C/L is also smaller than for typical parallel electrodes. Therefore, for the same device length, these modulators have capacitance comparable to that for parallel electrodes [53].

The modal birefringence of GaAs waveguides can be made very small and a uniform or very course period ($\sim$ mm) electrode can be used for TE $\leftrightarrow$ TM modulators. Therefore, the electrode configuration of Fig. 9, with the electrode parallel to the (110) plane, is appropriate [35].

To effect intensity modulation either a polarizer or a polarization splitter [54] must be integrated after the polarization modulator [115]. Effective polarizers can be made with metallic overlays for both $LiNbO_3$ [55] and GaAs waveguides [56]. Alternately, a single device in which TE $\leftrightarrow$ TM conversion is effected between a pair of mismatched coupled waveguides can be used [57].

For generality, we have examined above the bandwidth of the modulated parameter $\Delta\beta$. Of course, the intensity modulation bandwidth is the more important and directly measured quantity. For interferometric modulators whose intensity modulation is a known function of the integrated $\Delta\beta$, the expected intensity modulation bandwidth can be calculated using the frequency response of $\Delta\beta$ and (28). The voltage response of the directional coupler for nonuniform $\Delta\beta$ is not given simply by (25) with $\Delta\beta$L replaced by its integrated value and the intensity modulation bandwidth must generally be calculated numerically. However, in either casse, the bandwidth of $\Delta\beta$ is a good approximation to that of the resulting modulation. If, for analog applications, the modulators are biased for $\eta=0.5$ and only small signal modulated, intensity modulation is linear in $\Delta\beta$ and the intensity modulation bandwidth is the same as that for $\Delta\beta$.

VIII. Summary of Reported Modulator Results

Each of the above intensity modulators has been demonstrated. We survey some of the most significant results. A more complete survey of early modulators, as well as the various methods for measuring bandwidth, is given in [6]. We consider lumped and traveling-wave modulators separately. We quote the low frequency (generally $f=0$) modulation voltage reported and note that the modulation depths are not necessarily the same. The quoted bandwidths are for a 50Ω termination.

A $\sim$1-cm-long six-section reversed $\Delta\beta$ Ti:$LiNbO_3$ modulator at $\lambda=0.6328$ μm exhibited 1-GHz bandwidth for a modulation voltage of 3 V (using the weaker r_{13} coefficient) [58]. Similar results have been achieved at $\lambda=1.15$ μm using uniform mismatch electrodes [59]. An attempt to optimize $V/\Delta f$ by minimizing the waveguide mode size ($1-\mu$m Ti strip width) and using a small interelectrode gap (1 μm) is described in [33]. The 0.075-cm-long directional coupler modulator could be modulated with $\sim$6 V at $\lambda=0.6328$ μm and exhibited a switching time of $\sim$110 ps ($\sim$4 GHz). While this corresponds to a voltage$\cdot$length product of $\sim$0.5 V$\cdot$cm, the achieved bandwidth was below the potential bandwidth of $\sim$10 GHz. The $V/\Delta f$ value for the first two is $\sim$3 V/GHz while the latter is $\sim$1.5 V/GHz.

Recently a two-section $\Delta\beta$ reversed dc modulator was reported with measured bandwidth of 2.5 GHz at $\lambda=1.06$ μm for $V=4$ V and an electrode length of 0.9 cm [60]. This appears to be better than the expected optimum bandwidth performance for this electrode length. However, the two electrode sections were driven separately each with its own 50-Ω termination. Therefore, the effective length for determining the capacitance is 0.45 cm. The penalty, of course, if one drives each of these terminated electrodes from a common source, is that for broadband operation the source power must be four times larger than that applied to each electrode section. Therefore, the effective drive voltage is 8 V and $V/\Delta f=3.2$ V/GHz. All these modulators use the push-pull configuration of Fig. 10(a) or

(b), with electrodes on top the waveguides.

Several interferometric modulators have been reported, all using titanium diffused lithium niobate waveguides. A Y-branch modulator with the three electrode configuration in Fig. 10(c) (except with electrodes along side the waveguides) has been reported with $L = 0.6$ cm and a modulation voltage of 3.8 V at $\lambda = 0.647$ μm for a 9-μm gap [61]. The measured bandwidth was 1.1 GHz or $V/\Delta f = 3.45$ V/GHz.

In another interferometer without push-pull and with the configuration of Fig. 3(a), a modulation voltage of 4.4 V was achieved for an electrode length of 0.3 cm at $\lambda = 0.6328$ μm [62]. The bandwidth was not measured but the voltage length product of 1.32 V·cm is quite good.

Recently, a 1-GHz bandwidth TIR modulator has been reported, although the switching voltage for the device was not given [63]. A 1.7-GHz bandwidth has been achieved with a Ti:$LiNbO_3$ polarization modulator at $\lambda = 0.6$ μm [53]. The interaction length was 0.2 cm and the required drive 6 V, so $V/\Delta f = 3.5$ V/GHz.

There have been several semiconductor waveguide directional coupler switches reported. In an early GaAs metal-gap waveguide (Fig. 1(c)) directional coupler a 100-MHz bandwidth was measured for a 0.7-cm-long device which required ~25-volt modulation voltage [9]. However, the electrode had not been designed for low capacitance. Other more recent modulators exhibit switching voltages of 15–25 V for 0.8–1.1-cm electrode lengths [64]–[66]. No measured bandwidths were reported but capacitance values (measured for fix bias) indicate the *RC* potential for multigigahertz operation. The evaluation wavelengths for these devices was $\lambda = 1.06$ or 1.15 μm.

Currently, the most promising GaAs waveguide modulator, with respect to drive voltage, is the double-heterostructure polarization modulator. Nearly complete TE $\leftrightarrow$ TM conversion was achieved with ~10 V for a 0.1-cm-long electrode at $\lambda = 1.06$ μm. The measured capacitance of ~1 pF indicates a potential bandwidth of ~5 GHz or $V/\Delta f \simeq 2$ V/GHz [35]. Similar values of $V/\Delta f$ have been estimated for a recently reported polarization modulator which uses multiple electrodes to overcome the small waveguide birefringence in $Al_xGa_{1-x}As$ rib waveguides [67].

The first directional coupler modulators using waveguides on InP substrates have just been reported. For a 0.8-cm-long rib waveguide coupler, a 12-V modulation was required [68]. Good (16-dB extinction) crossover and straight through states could be achieved with the reversed $\Delta\beta$ coupler. A uniform $\Delta\beta$ coupler using Ge-diffused waveguides has also been reported [17]. A low switching voltage (~5 V) was achieved for the short ($L = 0.2$ cm) device, but the zero-voltage crossover efficiency was also small.

A Ti:$LiNbO_3$ traveling-wave dc modulator has been demonstrated at $\lambda = 1.32$ μm, an important wavelength for lightwave systems. The 1.6-cm-long electrode with $W = 14$ μm and $G = 6$ μm had a 35-Ω impedance [29]. Complete modulation could be achieved with a ~4-V swing. The measured bandwidth of 3.6 GHz corresponds to $V/\Delta f = 1.1$ V/GHz.

The fastest modulator reported to date uses a 50-Ω, 0.6-cm-long traveling-wave electrode on a Ti:$LiNbO_3$ Y-branch interferometer [24]. The 32-μm electrode gap allows the use of push–pull effect between the similarly separated interferometer arms (Fig. 13). However, because of the large gap, 8.8 V was required for 98-percent modulation efficiency at $\lambda = 0.6328$ μm. The measured bandwidth of 11.2 GHz yields $V/\Delta f = 0.8$ V/GHz. The 3-μm-thick, 20-μm-wide asymmetric coplanar strip electrode exhibited microwave insertion loss below 3 dB at 10 GHz.

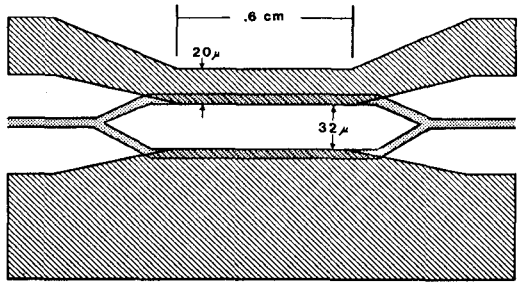

Fig. 13. Y-branch traveling-wave modulator ([24]).

The $V/\Delta f$ figure of merit is a valid means of comparing the above modulators for the same optical wavelength. When comparing modulator results for different wavelengths, a scale factor of $(\lambda_{1/\lambda_2})^q$, where q is between 1 and 2, is appropriate. For given $V/\Delta f$, reduced drive voltage can be achieved with the penalty of reduced bandwidth by using a longer electrode provided that electrical loss is not the limiting factor. To attain the potential tradeoff of voltage for bandwidth by using a shorter electrode also requires good microwave engineering to ensure high coax-electrode coupling and low loss at the higher frequencies.

A. Other Design Considerations

Other considerations besides modulation voltage and bandwidth may be equally important for practical application of these devices. In single-mode lightwave systems, for example, the fiber-coupled optical insertion loss is very critical. Recently, there has been considerable progress in this area for Ti:$LiNbO_3$ devices.

Loss contributions include fiber-waveguide coupling, reflection, propagation (both absorption and scattering), waveguide bend, and electrode loading. Reflection losses can be reduced with index-matching materials or antireflection coatings. Electrode loading losses, for the configuration of Fig. 3b, can be reduced with an intermediate dielectric buffer layer. There is some reduction in the effective voltage in the waveguide region, however, and there can be drift problems if the layer is not a good insulator.

Waveguide bends are necessary in several intensity modulators and are also required for integration [69]. Work toward reducing bend loss has concentrated on determining bend geometries which minimize loss for a given bend angle and maximizing mode confinement to increase the guided-wave's ability to negotiate bends. Bend losses as low as 0.3 dB [70] and 0.2 dB [71] have been achieved with S-shaped transitions for a lateral offset of 100 μm over a ~3-mm length for $\lambda = 0.63$ μm and $\lambda = 1.32$ μm, respectively. Using coherent coupling effects, a loss of only 6 dB was measured at $\lambda = 0.63$ μm for a semicircular waveguide consisting of 60 1° bends separated by the coherent cou-

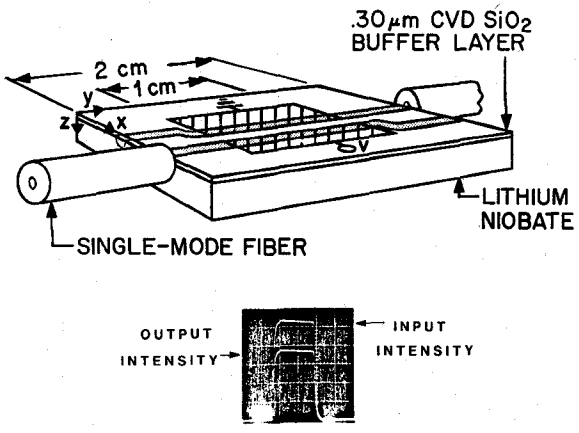

Fig. 14. Low-loss directional-coupler modulator coupled to single-mode fibers. The insert shows the on-state fiber-device-fiber loss of ~1.5 dB.

pling length of 180 μm [72]. The above results are for Ti:$LiNbO_3$ waveguides. Because of the larger guide-substrate index difference achievable in GaAs waveguides, bend losses in the latter can be quite low [73].

Fiber-waveguide coupling loss is due to misalignment and mismatch between the fiber and waveguide modes. The latter can be especially difficult because the fiber mode is symmetric while the waveguide mode (assuming an air cover) is asymmetric (Fig. 2). Nevertheless, with appropriate care, good fiber-waveguide coupling can be achieved. At $\lambda = 0.6328$ μm [74] and $\lambda = 1.15$ μm, [75] ~3-dB insertion loss has been achieved for coupling from a single-mode fiber to a Ti:$LiNbO_3$ waveguide, propagation through the 1-cm-long waveguide and coupling back to an identical fiber. By carefully tailoring the waveguide mode size to match that of the fiber, fiber-waveguide-fiber insertion loss of ~1 dB has been achieved at 1.3 μm for a waveguide of similar length [76]. In another approach, a fiber-waveguide coupling loss of ~0.2 dB has been attained by using a fiber tapered to match the waveguide mode [77]. The above results are for z-cut crystal; generally poorer results have been achieved for other orientations apparently of strong modal asymmetry [75].

The insertion loss of early modulators was very high or not reported. The traveling-wave directional coupler modulator at $\lambda = 1.32$ μm exhibited a fiber-device-fiber insertion loss of 5.4 dB at $\lambda = 1.32$ μm [29]. Somewhat lossier results have been achieved for $\lambda = 0.83$ μm with pig-tailed fibers [78]. By using waveguides well-matched to the fiber, a geometry which minimized the effect of bend loss and an effective buffer layer, a Ti:$LiNbO_3$ directional coupler modulator has recently been fabricated that exhibits total fiber-device-fiber insertion loss as low as 1.5 dB at $\lambda = 1.32$ μm [79]. A schematic of the device, whose total length is 2 cm, is shown in Fig. 14. Also shown is the measured relative intensity from the input fiber and intensity from the output fiber for the on state ($V = 0$).

The small mode size essential for efficient modulators and low-loss waveguide bends is generally incompatible with the relatively large mode sizes required for coupling to typical single-mode fibers [79]. Consequently, waveguide tapers will probably be needed to simultaneously optimize device performance and minimize fiber-waveguide loss. This problem, although very severe for the small mode size of semiconductor modulators, can be significantly overcome by integrating the modulator onto the laser chip.

There are several areas of waveguide modulator research where potential problems exist or where more data is needed. Perhaps foremost is the question of optical damage or photorefractive effect—an optical intensity dependent change in refractive index which occurs in $LiNbO_3$. The problem is acute at visible wavelengths. Indications point to orders of magnitude less sensitivity in the infrared, [80] but careful experiments at $\lambda = 1.3$ μm are needed. Questions of the long term stability to applied fields in lithium niobate need also be addressed.

Unwanted planar guiding for the extraordinary polarization apparently due to Li out diffusion plagued early strip-waveguide modulators [81]. Several techniques to eliminate this problem have been reported [82]–[87]. While each is apparently effective when properly applied, there seems to be some difficulties encountered when transferring these techniques to other laboratories.

Finally, short-term drift due to charge leakage through the dielectric buffer layer has been reported as a potential problem for low-frequency operation [88]–[90]. Buffer layers that allow dc operation have been achieved by oxidizing the SiO_2 [88] or Al_2O_3 film and by using chemical vapor deposited SiO_2 [91]. Alternately, the buffer layer can be etched away in the gap between the electrodes [92].

B. Applications

Waveguide modulators are very attractive for signal encoding in high bandwidth lightwave systems. While direct current modulation of the semiconductor laser sources is adequate for low bit rates, spectral spreading and hopping in typical lasers results in pulse spreading and reduced system bandwidth at high data rates (>0.5–1-Gbit/s) [93]. Furthermore, direct modulation above several gigahertz is inefficient. Other solutions to the first problem are under investigation—single longitudinal lasers like the Bragg [94] and short-cavity laser [95] and fibers with near zero dispersion over a broad spectral range [96]. However, external waveguide modulators also appear well-suited to solve this problem. External modulators may be essential for very high bandwidth ($\gtrsim$2 GHz) systems.

High-speed switches can be used for time-division multiplexing or gating in wide bandwidth lightwave systems. Such devices could interleave several relatively low data rate channels, each of which could be handled by conventional electronics, onto a single fiber. Gating of short pulses with a Ti:$LiNbO_3$ traveling-wave directional coupler has been demonstrated at a 1-GHz rate [97]. Several waveguide modulators, such as the Ti:$LiNbO_3$ TE⟨−⟩TM device, and the tunable directional coupler filter [98], are wavelength selective. These devices can be used to simultaneously perform signal encoding (modulation) and wavelength multiplexing functions.

For heterodyne systems, optical frequency shifting to match the local oscillator and the received signal frequencies may be necessary. A novel, parallel Y-branch single-sideband modulator with 2-GHz bandwidth has been reported which can perform this function [99].

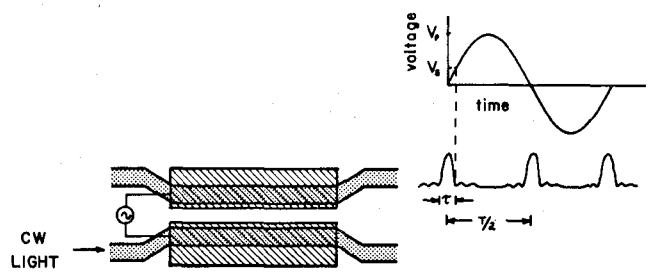

Fig. 15. Directional coupler as a high-speed gate or pulse generator. The horizontal axis represents the time light enters the coupler. The device is assumed to be velocity-matched.

Generally, modulators work well for a single linear polarization only. This can be a problem when used with typical fibers that do not preserve polarization. Specially designed Y-branch [89] and directional-coupler [100] modulators which can be used effectively with light of arbitrary polarization have been demonstrated.

Optical waveguide modulators are attractive for signal-processing applications. Low-speed phase modulators have been proposed for use in the integrated optic-processing chip for the fiber gyroscope [101]. High-speed analog-to-digital conversion can be performed with waveguide modulators [103]. A four-bit 830 megasample/s device has recently been reported [102]. The device uses a parallel array of four Y-branch interferometers with electrode lengths of even integer ratio. A/D conversion is achieved from the inteferometer's periodic voltage response ((28)). An interesting review of interferometric modulator applications in signal processing is given in [104].

The nonlinear voltage response of waveguide modulators can be used as the basis of hybrid bistable devices [105]. An interesting example is the optically controlled switch that uses a Ti: $LiNbO_3$ directional coupler [106], [107].

Two special purpose modulators have recently been proposed-to perform very high-speed sampling, multiplexing or short-pulse generation. These devices generate optical signals with very broad effective bandwidth (short pulses) in spite of being driven by only a single RF frequency. The price paid in each case is a peak drive voltage substantially larger than is needed to merely switch the modulator on and off.

One proposal, which uses a directional coupler with $L = l$, is shown schematically in Fig. 15 [101]. To describe its operation, we assume for the moment that the device is velocity matched. In this case, according to (19), there is a one-to-one correspondence between the time light enters the coupler and the constant voltage it sees along the length of the coupler. Light that enters when $V = 0$ couples to the second waveguide. However, light that enters the coupler at times such that $|V| > |V_S|$ (Fig. 15), where V_S is the switching voltage, mostly remains in the incident waveguide. Thus, light couples between the waveguides during each of the two voltage-zero crossings per RF period for a time interval that is, $\tau \sim (V_S/V_P)\ (T/2)$ (Fig. 15). To achieve short pulses or sampling intervals, a small T and V_S and large V_P are required. A long electrode is needed to achieve small V_S; for long electrodes, however, modulation

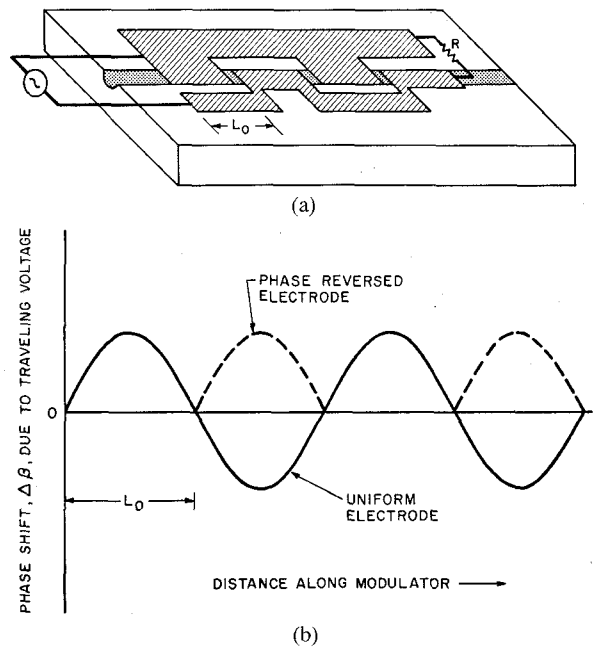

Fig. 16. (a) Velocity matching using periodic phase reversal. (b) The phase reversal length, L_0, is chosen to compensate for the voltage polarity reversal due to walkoff between the RF and optical signals. The solid curve represents relative $\Delta\beta$ seen along the modulator by light that enters the modulator at a particular time. Although shown for a single waveguide, the same technique can be used for a directional coupler.

at high frequency is possible only for the velocity-matched case. Otherwise, velocity matching is not essential and substantial compression ($\sim \tau/T$) can be achieved at low-pulse repetition rates without it. For a 10-GHz drive frequency, a pulse width less than ~ 1 ps is predicted for a velocity-matched allowable length of ~ 5 cm for $V_p \sim 10$ V (ignoring microwave loss) in lithium niobate.

In another proposal, the directional coupler is replaced by a cascade of interferometers [109]. Because of its periodic voltage response, an interferometer driven by a RF signal of frequency f and peak voltage $V = mV_S$ produces an optical signal modulated at a frequency mf, i.e., frequency multiplication results [62]. Each interferometer of the cascade is driven with a sinusoidal signal of frequency f but with peak voltage in the ratio 1, 2, 4, etc. The resulting optical signal is a train of pulses with repetition rate $2f$ and pulse width $\tau \sim (V_S/V_P)(T/2)$, where V_P is the maximum drive voltage. The interferometer cascade generates the harmonics necessary to form the pulse train. Because of the directional coupler's passband rather than periodic voltage response, this single device in the above proposal performs the same function as interferometer cascade.

For optimum performance, both devices require strong overdriving but only at a single, preferably high, frequency. In this case, so called artificial velocity-matching techniques can be very useful. Several such techniques have been proposed for bulk modulators. One technique proposed for guided-wave devices uses intermittent interaction between the RF and optical signals by periodically removing the electrode from the waveguide [109], [110].

Another approach which does not require such excess electrode length is shown in Fig. 16 [111]. Here the electrode is shifted at intervals

$$L_0 = \frac{\lambda_m}{2N_m}\left(1-\frac{N_0}{N_m}\right)^{-1} \tag{33}$$

equal to the walk-off length at the RF frequency of interest. This electrode shift reverses the direction of the applied field in the waveguide. This effective field reversal compensates exactly for the change in polarity of the applied voltage due to walk-off as shown in Fig. 16(b). However, velocity matching is achieved perfectly only for the design frequency. The bandwidth is still given approximately by (21) but the band has been displaced to higher frequencies. There are strong analogies between velocity-matching described here and the phase (or velocity) matching between two optical waves by periodic coupling as in the TE $\leftrightarrow$ TM modulator of Fig. 12(a).

IX. Summary

Optical waveguide modulator research has progressed rapidly in the last several years. The reports of high-performance modulators from laboratories around the world are indicative of the interest in the field. The significant efforts expended towards solving practical problems (such as insertion loss) are evidence of the expectations that these devices will play a significant role in future lightwave systems. We have reviewed the current status of the field with emphasis on design considerations for optimizing overall device performance.

Much work remains to be done. A thorough understanding of waveguide technology is important for optimizing modulator performance consistent with system requirements. Studies of long-term device characteristics are needed. Careful consideration of the design tradeoffs should result in reducing the drive-voltage requirements for traveling-wave modulators whose bandwidth potential has already been demonstrated. Electrooptic materials with better coefficients could reduce device length and the voltage/bandwidth radio. New modulator applications remain to be identified and explored. In the area of semiconductor modulators, investigation of traveling-wave structures should be fruitful. Most importantly, monolithic optical and optoelectronic integration offers challenging research opportunities and rewarding system applications.

Acknowledgment

It is a pleasure to acknowledge useful discussions with I. P. Kaminow, P. L. Liu, E. A. J. Marcatili, F. K. Reinhart, S. K. Korotky, and C. Joyner. I especially thank D. Marcuse for performing the numerical calculations of Fig. 4 and L. L. Buhl for assistance in preparing the manuscript.

References

[1] H. Kogelnik, "An introduction to integrated optics," *IEEE Trans. Microwave Theory Tech.*, vol. MTT-23, pp. 2–16, 1975.
[2] P. K. Tien, "Integrated optics and new wave phenomenon in optical waveguides," *Rev. Mod. Phys.*, vol. 49, pp. 361–381, 1977.
[3] H. F. Taylor and A. Yariv, "Guided wave optics," *Proc. IEEE*, vol. 62, pp. 1044–1060, 1974.
[4] I. P. Kaminow, "Optical waveguide modulators," *IEEE Trans. Microwave Theory Tech.*, vol. MTT-23, pp. 57–70, 1975.
[5] R. V. Schmidt and R. C. Alferness, "Directional coupler switches, modulators, and filters using alternating $\Delta\beta$ techniques," *IEEE Trans. Circuts Syst.*, vol. CAS-26, pp. 1099–1108, 1979.
[6] R. C. Alferness, "Guided-wave devices for optical communication," *IEEE J. Quantum Electron.*, QE-17, pp. 946–959, 1981.
[7] F. J. Leonberger, J. P. Donnelly, and C. O. Bozler, "GaAsP$^+$ n$^-$ n$^+$ directional-coupler switch," *Appl. Phys. Lett.*, vol. 29, pp. 652–654, 1976.
[8] J. C. Shelton, F. K. Reinhart, and R. A. Logan, "GaAs-Al$_x$ Ga$_{1-x}$As rib waveguide switches with MOS electrooptic control," *Appl. Opt.*, vol. 17, pp. 2548–2555, 1978.
[9] J. C. Campbell, F. A. Blum, D. W. Shaw, and K. C. Lawley, "GaAs electrooptic directional-coupler switch," *Appl. Phys. Lett.*, vol. 29, pp. 203–205, 1975.
[10] R. V. Schmidt and I. P. Kaminow, "Metal diffused optical waveguides in $LiNbO_3$," *Appl. Phys. Lett.*, vol. 25, pp. 458–460, 1974.
[11] H. Kogelnik and V. Ramaswamy, "Scaling rules for thin-film dielectric waveguides," *Appl. Opt.*, vol. 13, pp. 1857–1862, 1974.
[12] M. L. Shah, "Optical waveguides in $LiNbO_3$ by ion exchange techniques," *Appl. Phys. Lett.*, vol. 26, pp. 652–653, 1975.
[13] J. L. Jackel, "Optical waveguides in $LiTaO_3$: Silver lithium ion exchange," *Appl. Opt.*, vol. 19, pp. 1996–1999, 1980.
[14] F. J. Leonberger, C. O. Bozler, R. W. McClelland, and I. Melngailia, "Oxide-confined GaAs optical waveguides formed by lateral epitaxial growth," presented at the Topical Meeting Integrated Guided-Wave Opt., (Incline Village, NV), Jan. 18–20, 1980, Paper WB1.
[15] T. M. Benson, T. Murotani, P. N. Robson, and P. A. Houston, "Phootelastic optical waveguiding in InP epitaxial layers," presented at 7th Euro. Conf. on Optical Communication, (Copenhagen, Denmark), Sept. 8–11, 1981, Paper 9.4.
[16] N. L. DeMeo, F. J. Leonberger, and S. H. Groves, "Single-mode GaInAsP optical waveguides," presented at the Topical Meeting Integrated Guided-Wave Opt., (Asilomar, CA), Jan. 6–8, 1982, Paper WD7.
[17] I. P. Kaminow, R. C. Alferness, L. W. Stulz, and A. G. Dentai, "Optical waveguides in InGaAsP and InP by metal diffusion," presented at the Topical Meeting Integrated and Guided-Wave Opt., (Asilomar, CA,) Jan. 6–8, 1982, Paper WD6.
[18] I. P. Kaminow, *An Introduction to Electrooptic Devices*. New York: Academic Press, 1974.
[19] K. Tada and N. Suzuki, "Electrooptic coefficient of InP," *Japan J. Appl. Phys.*, vol. 19, pp. 2295–2297, 1980.
[20] Y. Yamamoto, T. Kamiya, and H. Yanai, *IEEE J. Quantum Electron.*, QE-11, pp. 729–736, 1975.
[21] D. Marcuse, "Optical electrode design for integrated optics modulators," *IEEE J. Quantum Electron.*, QE-18, pp. 393–398, 1982.
[22] D. G. Ramer, "Integrated optic electrooptic modulator electrode analysis," *IEEE J. Quantum Electron.*, QE-18, pp. 386–392, 1982.
[23] P. L. Liu, to be published.
[24] T. Sueta and M. Izutsu, "High-speed guided-wave optical components," presented at IOOC '81, (San Francisco, CA), Apr. 27–29, 1981, Paper TUM 2.
[25] J. S. Wei, "Distributed capacitance of planar electrodes in optical and acoustic surface wave devices," *IEEE J. Quantum Electron.*, QE-13, pp. 152–158, 1977.
[26] The frequently used expression, $C/_L = (2\varepsilon_{\text{eff}}/\pi)ln(4W/G)$ is a good approximation for the geometric dependence given in (10).
[27] F. Auracher and R. Keil, "Desing considerations and performance of Mach–Zehnder waveguide modulators," *Wave Electronics*, vol. 4, pp. 129–140, 1980.
[28] M. Izutsu, Y. Yamane, and T. Sueta, "Broad-band traveling-wave modulator using $LiNbO_3$ optical waveguide," *IEEE J. Quantum Electron.*, QE-13, pp. 287–290, 1977.
[29] K. Kubota, J. Noda, and O. Mikami, "Traveling-wave optical modulator using directional coupler $LiNbO_3$ waveguide," *IEEE J. Quantum Electron.*, QE-16, pp. 754–760, 1981.
[30] K. C. Gupta, R. Garg, and I. J. Bahl, *Microstrip Lines and Slotlines*. Washington: Artech, 1979.
[31] D. W. Widmann, "Metalization for integrated circuits using a lift-off technique," *IEEE J. Solid-State Circuits*, SC-11, pp. 446–471, 1976
[32] P. L. Liu, to be published.

[33] R. C. Alferness, N. P. Economou, and L. L. Buhl, "Fast compact optical directional coupler switch/modulator," *Appl. Phys. Lett.*, vol. 38, pp. 214–216, 1981.

[34] P. M. Schaible, W. C. Metzger, and J. P Anderson, "Reactive ion etching of aluminum and aluminum alloys in an RF plasma containing halogen species," *J. Vac. Sci. Technol.*, vol. 15, pp. 334–337, 1978.

[35] J. McKenna and F. K Reinhart, "Double-heterostructure $GaAsAl_xGa_{1-x}$ 110 p-n-junction-diode modulator," *J. Appl. Phys.*, vol. 47, p. 2069, 1976.

[36] E. S. Yang, *Fundamentals of Semiconductor Devices*. New York: McGraw-Hill, 1978.

[37] F. K. Reinhart, "Reversed-biased giallium phosphide diodes as high-frequency light modulators," *J. Appl. Phys.*, 39, pp. 3426–3434, 1968.

[38] M. Papuchon *et al.*, "Electrically switched optical directional coupler: COBRA," *Appl. Phys Lett*, vol. 27, pp. 289–291, 1975.

[39] E. A. J. Marcatili, "Dielectric Waveguides," *Bell Syst. Tech. J.*, vol. 48, pp. 2071–2102, 1969.

[40] R. C. Alferness, R. V. Schmidt, and E. H. Turner, "Characteristics of Ti-diffused $LiNbO_3$ optical directional couplers," *Appl. Opt*, 18, pp. 4012–4018, 1979.

[41] H. Kogelnik, "Theory of dielectric waveguides," in *Integrated Optics*, T. Tamir, Ed., New York: Springer–Verlag, 1975.

[42] R. C. Alferness and P. S. Cross, "Filter characteristics of codirectionally coupled waveguides with weighted coupling," *IEEE J. Quantum Electron.*, vol. QE-14, pp. 843–847, 1978; R. C. Alferness, "Optical directional couplers with weighted coupling," *Appl. Phys. Lett.*, vol. 35, pp. 260–262, 1979

[43] H. Kogelnik and R. V. Schmidt, "Switched directional couplers with alternating $\Delta\beta$," *IEEE J. Quantum* Electron., vol. QE-12, pp. 396–401, 1976.

[44] R. V. Schmidt and H. Kogelnik, "Electrooptically switched coupler with stepped $\Delta\beta$ reversal using Ti-diffused $LiNbO_3$ waveguides," *Appl. Phys. Lett.*, vol. 2, pp. 503–505, 1976.

[45] W. E. Martin, "A new waveguide switch/modulator for integrated optics," *Appl. Phys. Lett.*, vol. 26, pp. 562–563, 1975.

[46] V. Ramaswamy, M. D. Divino, and R. D. Standley, "A balanced bridge modulator switch," *Appl. Phys. Lett.*, vol. 32, pp. 644–646, 1978.

[47] M. Minakata, "Efficient $LiNbO_3$ balanced bridge modulator/switch with ion-etched slot," *Appl. Phys. Lett.*, vol. 35, pp 40–42, 1979

[48] O. Mikami and S. Zembutsu, "Modified balanced-bridge switch with two straight waveguides," *Appl. Phys. Lett.*, vol. 35, pp. 145–147, 1978.

[49] A. Neyer and W. Sohler, "High-speed cutoff modulator using a Ti-diffused $LiNbO_3$ channel waveguide," *Appl. Phys. Lett.*, vol. 35, pp. 256–258, 1979.

[50] C. S. Tsai, B. Kim, and F. R. EL-Akkari, "Optical channel waveguide switch and coupler using total internal reflection," *IEEE J. Quantum Electron.*, QE-14, pp. 513–517, 1978.

[51] A. Yariv, "Coupled-mode theory for guided-wave optics," *IEEE J. Quantum Electron.*, vol. QE-9, pp. 919–934, 1973.

[52] R. C. Alferness, "Efficient waveguide electrooptic TE $\leftrightarrow$ TM mode converter/wavelength filter," *Appl. Phys. Lett.*, vol. 36, pp 513–515, 1980.

[53] R. C. Alferness and L. L. Buhl, "High-speed waveguide electro-optic polarization modulator," to be published in *Opt. Lett*

[54] O. Mikami, "$LiNbO_3$ coupled-waveguide TE/TM mode splitter," *Appl. Phys. Lett.*, vol. 36, pp. 491–493, 1980.

[55] T. Findakly and C. L. Chen, "Diffused optical waveguides with exponential profile: Effects of metal-clad and dielectric overlay," *Appl. Opt.*, vol. 17, pp. 469–473, 1978.

[56] F. K. Reinhart, J. C. Shelton, R. A. Logan, and B. W. Lee, "$GaAs_yGa_{1-y}As$ single heterostructure MOS rib waveguide polarizer," *Appl. Phys. Lett.*, vol. 36, pp. 237–140.

[57] R. C. Alferness and L. L. Buhl, "Polarization-independent optical filters using interwaveguide TE $\leftrightarrow$ TM conversion," *Appl. Phys. Lett.*, vol. 39, pp. 131–134, 1981.

[58] P. S. Cross and R. V. Schmidt, "A 1 Gbit/s integrated optical modulator," *IEEE J. Quantum Electron.*, vol. QE-15, pp. 1415–1418, 1978.

[59] O. Mikami, J. Noda, and M. Fukuma, "Directional coupler type light modulator using $LiNbO_3$ waveguides," *Trans IECE Japan*, vol E-61, pp. 144–147, 1978.

[60] P. Thioulouse, A. Carenco, and R. Guglielmi, "High-speed modulation of an electrooptic directional coupler," *IEEE J. Quantum Electron.*, QE-17, pp. 535–541, 1981.

[61] F. Auracher and R. Keil, "Method for measuring the RF modulation characteristics of Mach–Zehnder-type modulators," *Appl. Phys Lett.*, vol. 36, pp. 626–629.

[62] F. J. Leonberger, "High-speed operation of $LiNbO_3$ electrooptic interferometric waveguide modulators," *Opt. Lett.*, vol. 5, pp. 312–314, 1980.

[63] C L Chang and C. S. Tsai, "GHz bandwidth optical channel waveguide TIR switches and 4×4 switching networks," presented at the Topical Meeting Integrated and Guided-Wave Opt (Asilomar, CA), 1982, Paper TuD2.

[64] A. Carenco, L Meniguax, and P. Delpech, "Multiwavelength GaAs rib waveguide directional coupler with stepped $\Delta\beta$ Schotky electrodes," *J. Appl. Phys.* vol 50, p. 5139, 1979.

[65] A. Carenco, L. Menigaux, F. Alexandre, M. Abdalla, and A. Brenac, "Directional coupler switch in molecular-beam epitaxy GaAs," *Appl. Phys. Lett.*, vol. 34, pp. 755–757, 1979.

[66] F. J. Leonberger and C. O. Bozler, "GaAs directional coupler switch with stepped $\Delta\beta$ reversal," *Appl. Phys.*, 31, pp. 223–225, 1977.

[67] F. K. Reinhart, R. A. Logan, and W. R. Sinclair, "Electrooptic polarization modulation in multielectrode $Al_xGa_{1-x}As$ rib waveguides," *IEEE J. Quantum Electron.*, vol. QE-18, pp. 763–766, 1982.

[68] L. Menigaux, A. Carenco, d N. T. Linh, "InP electrooptic directional coupler switch," presented at the Topical Meeting Integrated d Guided-Wave Opt., (Asilomar, CA), 1982, Paper TLD5.

[69] L. D. Hutcheson, I. A. White, and J. J. Burke, "Comparison of bending losses in integrated optical circuits," *Opt. Lett.*, vol. 5, pp. 276–278, 1980.

[70] V. Ramaswamy and M. D. Divino, "Low-loss bends for integrated optics," presented at Conf. on Lasers and Electrooptics, paper THP1, (Washington, DC), 1981.

[71] W. J. Minford and R. C. Alferness, "Low-loss Ti:$LiNbO_3$ waveguide bends at $\lambda = 1.3$ μm," presented at the Topical Meeting on Integrated and Guided-Wave Opt. (Asilomar, CA), 1982, Paper WD3, to be published in *IEEE J. Quantum Electron*, Sept. 1982.

[72] L. M. Johnson and F. J. Leonberger, "Low-loss $LiNbO_3$ waveguide bends with coherent coupling," presented at IOOC '81, (San Francisco, CA), 1981, Paper TuM1.

[73] M. W. Austin, "Curved rib waveguides in GaAs/GaAlAs," presented at First Euro. Conf. on Integrated Optics, (London), 1981.

[74] C. H. Bulmer, S. K Sheem, R. P. Moeller, and W. K Burns, "High efficiency flip-chip coupling between single-mode fibers and $LiNbO_3$ channel waveguides," *Appl. Phys. Lett.*, vol. 37, pp. 351–353, 1980.

[75] M. Kukuma and J. Noda, "Optical properties of Ti-diffused $LiNbO_3$ strip waveguides and their coupling-to-a-fiber characteristics," *Appl Opt.*, vol. 19, pp. 591–597, 1980.

[76] V. Ramaswamy, R. C. Alferness, and M. D. Divino, "High efficiency single-mode fiber to Ti:$LiNbO_3$ waveguide coupling," *Elect. Lett.*, vol. 18, pp. 30–31, 1982.

[77] M. Papuchon, P. Kayoun, and Y. Bourbin, "High coupling efficiency between single-mode optical fibers and Ti-diffused $LiNbO_3$," presented at the Topical Meeting on Integrated and Guided-Wave Opt. (Asilomar, CA), 1982, Paper FB3.

[78] O. G. Ramer, C. Nelson, and C. Mohr, "Experimental integrated optic circuit losses," *IEEE J. Quantum Electron.*, QE-17, pp. 970–974, 1981.

[79] R C. Alferness, L. L. Buhl, and M. D. Divino, "Low-loss fiber-coupled waveguide directional coupler modulator," *Elec.. Lett.*, vol. 18 pp. 490–491, 1982.

[80] R. V. Schmidt, P S. Cross, and A. M. Glass, "Optically induced crosstalk in $LiNbO_3$ waveguide switches," *J. Appl. Phys.*, vol. 51, pp. 90–93, 1980.

[81] T R. Ranganath and S. Wang, "Ti-diffused $LiNbO_3$ branched-waveguide modulators performance and design," *IEEE J. Quantum Electron.*, vol. QE-13, pp. 290–295, 1977.

[82] T. R. Ranganath and S. Wang, "Suppression of Li_2O out-diffusion from Ti-diffused $LiNbO_3$ optical waveguides," *Appl. Phys. Lett.*, vol. 30, pp. 376–379, 1977.

[83] B. Chen and A. C. Pastor, "Elimination of Li_2O out-diffusion waveguide in $LiNbO_3$ and $LiTaO_3$," *Appl. Phys. Lett.*, vol. 30, pp. 570–571, 1977.

[84] W. K. Burns, C. H. Bulmer, and E. J. West, "Application of Li_2O compensation techniques to Ti-diffused $LiNbO_3$ planar and channel waveguides," *Appl Phys Lett.*, 33, pp. 70–72, 1978.

[85] R. C. Alferness and L. L. Buhl, "Electrooptic waveguide TE ↔ TM mode converter with low drive voltage," *Opt. Lett.*, vol. 5, pp. 473–475, 1980.
[86] J. L. Jackel, V. Ramaswamy, and S. Lyman, "Elimination of out-diffused surface guiding in Titantium-diffused $LiNbO_3$," *Appl. Phys. Lett.*, 38, p. 509–510, 1981.
[87] R. J. Esdaile, *Appl. Phys. Lett.*, 33, pp. 733–735, 1978.
[88] G. L. Tangonan, D. L. Persechini, J. F. Lotspeich, and M. K. Barnoski, "Electrooptic diffraction modulation in Ti-diffused $LiTaO_3$," *Appl. Opt.*, vol. 17, pp. 3259–3263, 1978.
[89] W. K. Burns, T. G. Giallorenzi, R. P. Moeller, and E. J. West, "Interferometric waveguide modulator with polarization-independent operation," *Appl. Phys. Lett.*, vol. 33, pp. 944–947, 1978.
[90] P. L. Liu, "Space-charge effect in $LiNbO_3$ waveguide modulator," presented at the Topical Meeting on Integrated and Guided-Wave Optics, (Asilomar, CA), 1982, Paper FA2.
[91] R. C. Alferness and L. L. Buhl, "Waveguide electrooptic polarization transformer," *Appl. Phys. Lett*, vol. 38, pp. 655–657, 1981.
[92] S. Yamada and M. Minakata, "Drift in $LiNbO_3$ waveguide modulators," *Jap. J. Appl. Phys.*, vol. 20, pp. 733–737, 1981.
[93] T. Kimura, "Single-mode systems and components for longer wavelengths," *IEEE Trans. Circuits Syst.*, vol. CAS-26, pp. 987–1010, 1979.
[94] Y. Sakakibara, K. Furuya, K. Utaka, and Y. Suematsu, "Single-mode oscillation under high-speed direct modulation in GaInAsP/InP integrated twin-guide lasers with distributed Bragg reflectors," *Elect. Lett.*, vol. 16, pp. 456–458, 1980.
[95] C. A. Burrus, T. P. Lee, and A. G. Dentai, "Short cavity single-mode 1.3-μm InGaAsP lasers with evaporated high reflecting mirrors," *Elect. Letts.*, vol. 17, pp. 954–956, 1981.
[96] L. G. Cohen and W. L. Mammel, "Tailoring the shapes of dispersion spectra to control bandwidth in single-mode fibers," presented at 7th Euro. Conf. Opt. Comm., (Copenhagen), 1981, Paper 3.3.
[97] J. Noda, S. Tarucha, K. Kubota, and K. Otsuka, presented at Conf. on Lasers and Electrooptics, (Washington, DC), 1981, Paper THP2.
[98] R. C. Alferness and R. V. Schmidt, "Tunable optical waveguide directional coupler filter," *Appl. Phys. Lett.*, vol. 33, pp. 161–163, 1978.
[99] M. Izutsu, S. Shikama, and T. Sueta, "Integrated optical SSB modulator/frequency shifter," *IEEE J. Quantum Electron.*, QE-17, pp. 2225–2227, 1981.
[100] R. C. Alferness, "Polarization-independent optical directional coupler switch using weighted coupling," *Appl. Phys. Lett.*, vol. 35, pp. 748–750, 1979.
[101] H. Arditty and M. Papuchon, "Recent developments in guided-wave optical rotation sensors," presented at the Topical Meeting on Integrated and Guided-Wave Opt., (Incline Village, NV), 1980 Paper TuC2.
[102] F. J. Leonberger, C. E. Woodward, and R. A. Becker," 4-bit 828-megasample/s electrooptic guided-wave analog-to-digital converter," *Appl. Phys. Lett.*, vol. 40, pp. 565–568, 1982.
[103] H. F. Taylor, M. J. Taylor, and P. W. Bauer, "Electrooptic analog-to-digital conversion using channel waveguide modulators," *Appl. Phys. Lett.*, vol. 32, pp. 559–561, 1978.
[104] F. J. Leonberger, "Applications of guided-wave interferometers," *Laser Focus*, pp. 125–129, Mar. 1982.
[105] P. W. Smith, I. P. Kaminow, P. J. Maloney, and L. W. Stulz, "Integrated bistable optical devices," *Appl. Phys. Lett.*, vol. 33, pp. 24–26, 1978.
[106] P. S. Cross, R. V. Schmidt, R. L. Thornton, and P. W. Smith, "Optically controlled directional coupler switch," *IEEE J. Quantum Electron.*, QE-14, p. 577–579, 1978.
[107] A. Schnapper, M. Papuchon, and C. Puech, "Remotely controlled directional coupler switch," *IEEE J. Quantum Electron.*, vol. QE-17, pp. 332–335, 1981.
[108] E. A. J. Marcatili, "Optical subpicosecond gate," *Appl. Opt.*, vol. 19, pp. 1468–1476, 1980.
[109] H. Haus, S. Kirsch, K. Mathyssek, and F. J. Leonberger, "Picosecond optical sampling," *IEEE J. Quantum Electron.*, vol. QE-16, pp. 870–880, 1980.
[110] E. A. J. Marcatili, patent pending.
[111] P. L. Liu, "Recent developments in high-speed integrated optical gates," *J. Opt. Commun.*, Mar. 1981.
[112] R. C. Alferness, patent pending.
[113] I. P. Kaminow and L. W. Stulz, "Loss in cleaved Ti-diffused $LiNbO_3$ waveguides," *Appl. Phys. Lett.*, vol. 33, pp. 62–65, 1978.
[114] R. C. Alferness, V. Ramaswamy, S. K. Korotky, M. D. Divino, and L. L. Buhl, "Efficient single-mode fiber to Ti:$LiNbO_3$ waveguide coupling," *IEEE J. Quantum Electron.*, to be published, Sept. 1982.
[115] F. K. Reinhart, "Prospects of monolithic optical integration," in *Proc. SPIE*, vol. 272, pp. 66–75, 1980.

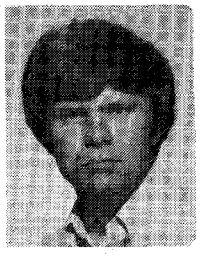

Rod C. Alferness received the B. S. degree in physics from Hamline University, St. Paul, MN, in 1968 and the M.S. and Ph.D. degrees in physics from the University of Michigan, Ann Arbor, MI, in 1970 and 1976, respectively. His thesis work was on optical diffraction in thick, holographic gratings.

From 1970 to 1972 he was a member of the U.S. Army stationed at Fort Monmouth, NJ, where he performed theoretical studies of laser propagation in the atmosphere. He joined Bell Laboratories, Holmdel, NJ, in June 1976, where he has been engaged in research on optical guided-wave devices including switches, modulators, wavelength filters and polarization controllers.